Characterization of reactive transport by 3D electrical resistivity tomography (ERT) under unsaturated conditions

Markus Wehrer[1*], Andrew Binley[2] and Lee D. Slater[3]

[1] Lehrstuhl für Hydrogeologie
Institut für Geowissenschaften
Friedrich-Schiller-Universität Jena
Burgweg 11
07749 Jena
Germany
*corresponding author: markus.wehrer@uni-jena.de

[2]Lancaster University
Lancaster Environment Centre,
Lancaster University,
Lancaster, LA1 4YQ,
United Kingdom

[3] Dept. of Earth and Environmental Sciences
Rutgers, The State University of New Jersey
101 Warren Street, Smith Hall, Room 135
Newark, NJ 07102
United States

Keypoints

- ERT shows the production of ions associated with nitrification resulting from a fertilizer application in a multicompartment lysimeter
- Shape measures of local breakthrough curves of nitrate and bulk conductivity observed by ERT are highly correlated
- ERT can be qualitatively and quantitatively informative with respect to processes affecting the fate of nitrate in arable soils

Abstract

The leaching of nitrate from intensively used arable soil is of major concern in many countries. In this study we show how time lapse electrical resistivity tomography (ERT) can be used to characterize spatially heterogeneous processes of ion production, consumption and transport in soils. A controlled release fertilizer was introduced into an undisturbed soil core in a laboratory lysimeter and subjected to infiltration events. The production of ions resulting from processes associated with nitrification and their transport through the soil core was observed by time lapse ERT and analysis of seepage water samples from a multicompartment sampler. ERT images show development and propagation of a high conductivity plume from the fertilizer source zone. Molar amounts of nitrate produced in and exported from the soil core could be well reproduced by time lapse ERT using a spatial moment analysis. Furthermore, we observed that several shape measures of local breakthrough-curves (BTCs) of seepage water conductivity and nitrate derived by effluent analyses and BTCs of bulk conductivity derived by ERT are highly correlated, indicating the preservation of spatial differences of the plume breakthrough in the ERT data. Also differences between nitrate breakthrough and a conservative tracer breakthrough can be observed by ERT. However, the estimation of target ion concentrations by ERT is errorbound and the smoothing algorithm of the inversion masks spatial conductivity differences. This results in difficulties reproducing spatial differences of ion source functions and variances of travel times. Despite the observed limitations, we conclude that time lapse ERT can be qualitatively and quantitatively informative with respect to processes affecting the fate of nitrate in arable soils.

Keywords

nitrate leaching, nitrogen cycle, time-lapse electrical resistivity tomography, ERT, multicompartment sampler, lysimeter

Index terms:

Hydrogeophysics; Vadose zone; Biogeophysics; Biogeochemical cycles, processes, and modeling; Instruments and techniques: Monitoring

1. Introduction

Intensive farming on arable soils is subjecting surface- and shallow groundwater bodies to high levels of dissolved nitrate due to the heavy use of nitrogen fertilizers. 15% of shallow groundwater samples exceeded the Nitrate-Directive limit of 50 mg/l nitrate in the EU27 member states in the monitoring period 2008-2011 [*European Commission*, 2011]. Large areas in the Midwest and northeast of the United States are also subject to a high risk of nitrate contamination of groundwater [*Dubrovsky et al.*, 2010]. 24% of the drinking water wells in these areas exhibit nitrate concentrations exceeding drinking water standards [*Nolan et al.*, 1998]. Leaching of nitrate with soil water is a major unintended loss of nitrogen from arable soils [*White and Sharpley*, 1996]. EU wide, 21% of the total nitrogen loss of soils is attributed to nitrate leaching [*Velthof et al.*, 2014]. *Van Breemen et al.* [2002] estimated the loss due to leaching to roughly 10-20% in several catchments in the NE of the US. Consequently, management practices are being developed and applied to reduce nitrate leaching. One example is the application of slow or controlled release fertilizers, which aims for a more efficient use of the nitrogen introduced into the soil [*Munoz et al.*, 2005; *Zebarth et al.*, 2012].

Due to the large spatio-temporal variability, leaching of nitrate and its export to surface waters by drainage and groundwater is one of several components of the nitrogen budget in soil that is difficult to quantify [*Bakhsh et al.*, 2010; *Marchetti et al.*, 2004; *Onsoy et al.*, 2005; *Van Breemen et al.*, 2002; *White and Sharpley*, 1996]. Production of nitrate depends on several consecutive rate-limited processes, such as transformation of organic N to nitrate in the nitrification chain [*Chien et al.*, 2011] and diffusive transport out of soil aggregates into mobile water [*Magesan et al.*, 1996]. Nitrate in the soil water may be decomposed by denitrification, which is again a rate-limited and spatially variable process [*Chien et al.*, 2011].

Transport of nitrate depends on soil water flow, which is a very complex process by itself, due to the ubiquitous presence of heterogeneous flow in the vadose zone [*Fluhler et al.*, 1996; *Hendrickx and Flury*, 2001]. Currently, the prediction of heterogeneous flow is still a major challenge, due to inappropriate conceptual models and limitations of measurement techniques providing the required data for model parameterization [*Beven and Germann*, 2013; *Gerke et al.*, 2010; *Simunek et al.*, 2003]. Depending on the conditions of nitrate availability and preferential flow

initiation, preferential flow may result in a reduction or enhancement of nitrate leaching [*Larsson and Jarvis*, 1999; *Macduff and White*, 1984]. Precipitation shortly after fertilizer application can result in large seepage water loads of nitrate, while macropore flow during winter bypasses the soil matrix, where the nitrate is stored, and thus reduces leaching [*Larsson and Jarvis*, 1999; *Macduff and White*, 1984]. Furthermore, there are feedback mechanisms between preferential transport pathways and microbial activity, because such pathways act as microbial hot spots [*Bundt et al.*, 2001] and in turn the microbial activity reinforces pathways, e.g. through precipitation of iron oxides along fringes of pathways [*Lissner et al.*, 2014; *Morales et al.*, 2010].

White and Sharpley [1996] come to the conclusion that the most reliable estimates of nitrate leaching come from fields with tile drains, where the load is integrated over the entire area. Yet, not every type of soil is suitable for tile drainage and alternative techniques need to be applied. *White and Sharpley* [1996] recommend suction samplers, but *Weihermuller et al.* [2007] point out that any sample taken at a specific location at a specific time with traditional soil solution sampling (by wick samplers, suction cups or -plates and lysimeters) is not representative of any other location or time at the scale of an agricultural field (or larger). *Weihermuller et al.* [2007] and *Kohne et al.* [2009] state that a combination of tomographic geophysical techniques and traditional soil and soil solution sampling techniques could solve this problem.

Considerable development in the field of electrical resistivity tomography for the characterization of solute breakthroughs has occurred over the last 20 years [*Binley et al.*, 1996; *Day-Lewis and Singha*, 2008; *French et al.*, 2002; *Garre et al.*, 2010; *Irving and Singha*, 2010; *Koestel et al.*, 2008; *Koestel et al.*, 2009b; *Koestel et al.*, 2009c; *Olsen et al.*, 1999; *Singha et al.*, 2007; *Slater et al.*, 1997; *Wehrer et al.*, 2014; *Wehrer and Slater*, 2015]. The potential of ERT to visualize heterogeneous conservative transport was shown by cross-borehole tomography [*Daily et al.*, 1992], 2D imaging along a trench [*French et al.*, 2002] and 3D imaging in lysimeters [*Binley et al.*, 1996; *Garre et al.*, 2010; *Koestel et al.*, 2008; *Olsen et al.*, 1999; *Wehrer et al.*, 2014; *Wehrer and Slater*, 2015]. Temporal and spatial moments derived from time-lapse images were validated for breakthroughs of conservative tracers [*French et al.*, 2002; *Koestel et al.*, 2009c; *Wehrer and Slater*, 2015] and show that quantitative information on transport processes can be extracted using this technique. Observation and validation of reactive tracer breakthroughs using ERT in the

unsaturated zone are rare [*Wehrer et al.*, 2014]. Observations of heterogeneous flow and transport done by ERT can be validated using dye tracer breakthroughs [*Binley et al.*, 1996; *Koestel et al.*, 2009a] or using a multicompartment sampler (MCS) [*Wehrer and Slater*, 2015]. In contrast to dye tracing techniques, the validation by MCS does not require destruction of the soil core. However, the MCS breakthrough data integrates over the entire path length, limiting the resolving power of processes occurring inside of the core [*Bloem et al.*, 2008].

The objective of this study is to show the potential of 3D ERT to characterize reactive heterogeneous transport in unsaturated media under partly transient conditions. In particular, we investigate whether ERT data can provide a quantitative basis for further analysis (e.g. by flow and transport modeling) of nitrogen fertilizer transformation and transport processes. This is performed by analyzing formation and transport of ions in a soil core, which is subject to heterogeneous flow conditions, in response to a controlled release fertilizer application in a laboratory lysimeter. The experiment was motivated by current research activities at the Cornell University Cooperative Extension of Suffolk County to address the nitrate problem in groundwater of Long Island (NY) [*Flipse and Bonner*, 1985] by the use of controlled release fertilizer in potato cropping [*Sanwald and Wiseman*, 2012, 2013]. We deliberately chose to allow for variations in water content as they would occur in response to precipitation in the field during the experiment, because preferential flow is often triggered in response to time variable infiltration [*Clothier et al.*, 2008; *Wang et al.*, 2003]. The lysimeter was equipped with a multicompartment suction plate, ERT electrodes for 3D time-lapse tomography, water content probes and tensiometers.

2. Materials and Methods

2.1. Lysimeter experiment

The experiment was carried out on a 0.48 m deep soil core contained in a laboratory lysimeter (0.5 m length, 0.5 m width, 0.6 m height). The setup of this lysimeter was described previously [*Wehrer and Slater*, 2015] and is only summarized here. An undisturbed soil core was retrieved from an agricultural field near Riverside, Long Island, NY, USA , with the procedure described in *Wehrer and Slater* [2015]. The site is subject to regular plowing, fertilization and other agricultural practices. A plow horizon was observed to a depth of 0.3 m, with a compacted zone around 0.3 m depth. Below the plow horizon follows a mineral subsoil. Both horizons have the same sandy silt texture with little clay (4%-6%). Detailed properties of the soil are published in *Wehrer and Slater* [2015]. The hydraulic and electrical properties of the soil material of the plow horizon were characterized in soil column experiments [*Grunat et al.*, 2013]. The lysimeter was equipped with water content probes (EC-5, Decagon Devices, Pullman, USA) and tensiometers (custom made, *Grunat et al.* [2013]) at 0.05 m, 0.22 m and 0.46 m depth as shown in Figure 1. Temperature was measured with a thermocouple (HEL-700 RTD, Digikey, Thief River Falls, USA), placed 2 cm below soil surface. Average temperature of the soil in the air conditioned laboratory was 22.7 °C with a standard deviation of 1.2 °C over the 12 month experimental period. We assumed a static, homogeneous temperature distribution inside the core over the experimental period, negating the need to correct ERT measurements for temperature variation.

The bottom of the soil core was equipped with a multicompartment sampler (MCS; Ecotech GmbH, Bonn, Germany) with 36 regularly spaced compartments (Figure 1). Aqueous samples were collected in 100 ml polyethylene bottles (Fisherbrand, Thermo-Fisher Scientific, USA). Electrical conductivity and nitrate concentrations (detection limit 0.56 mg/l) of the samples were analyzed as described in *Wehrer and Slater* [2015]. Electrical conductivity was analyzed in each sampling bottle and samples of each single infiltration of each compartment were combined to analyze nitrate. The lysimeter was equipped with 144 ERT electrodes (36 electrodes spaced 8.2 cm apart from each other on the four vertical sides of the core, Figure 1). The ERT electrodes were constructed with silver wires in KCl-Agar gel with electrolytic

188 contact to the soil. The details of the construction, including the sprinkler system, are
189 described in *Wehrer and Slater* [2015].

190

191 *Figure 1*

192

193 Twenty two infiltration events with durations between 2h and 5h, infiltration amounts
194 between 10.0 and 21.3 mm and rates between 3.1 and 6.9 mm h^{-1} were carried out,
195 mostly with pauses of one week in between (Table 1). This corresponds to medium
196 and high intensity precipitation events observed at the Brookhaven weather station
197 near the field site [*NOAA*, 2013] and mimics a more natural precipitation regime than
198 steady state flow. A total amount of 300 l m^{-2} was infiltrated over a one year period. A
199 controlled pressure of -50 hPa was applied to the bottom of the core, with the
200 exception of before the 3rd infiltration and until the 7th infiltration when the pressure
201 was decreased to -100 hPa. A 0.3 g l^{-1} $CaCl_2$ solution with a conductivity of σ_{in} = 545
202 µS cm^{-1} (=0.0545 S m^{-1}) was used as the background input solution. This is well
203 within the range of pore water conductivities present in agricultural soils [*Blume et al.*,
204 2010]. We used a divalent cation to avoid colloid mobilization [*McCarthy and McKay*,
205 2004]. Evaporation was reduced by covering the surface with a plastic sheet.

206

207 Table 1

208

209 *2.2. Fertilizer addition and transformations in the nitrogen cycle*

210 A polymer coated controlled release urea fertilizer (ESN 44-0-0, Agrium Inc., Denver,
211 US) was added to the soil core to investigate production and transport of nitrate. In
212 field trials, buried ESN 44-0-0 fertilizer released its complete amount of nitrogen
213 within 3 months [*Sanwald and Wiseman*, 2008]. This mode of application was based
214 on the field application procedure [*Sanwald and Wiseman*, 2012, 2013]. Two small
215 straight trenches (≈3 cm wide, 10 cm deep) were dug parallel to one another 6.3 cm
216 left and right from the center across the length of the core. A single straight line of
217 fertilizer granules (2.0 g N each line, equal to the amount used in the field for potato
218 cropping, in total 0.145 moles of urea or 0.290 moles of N) was distributed on the

bottom of each trench and soil was then used to fill up the trenches and slightly compressed by hand.

Microbial processes associated with the transformation of urea introduced with the fertilizer result in the production of charge carriers, primarily nitrate, protons and hydrogen carbonate, if the nitrification is complete. Thus, these processes influence the electrical conductivity of the soil solution. Urea in the soil is transformed into ammonia via hydrolysis by the urease enzyme [*Chien et al.*, 2011]:

$$(NH_2)_2CO + 2H_2O \rightarrow (NH_4)_2CO_3 \qquad \text{Equation 1}$$

$$(NH_4)_2CO_3 + H_2O \rightarrow 2NH_4^+ + HCO_3^- + OH^- \qquad \text{Equation 2}$$

Under oxidizing conditions, ammonia is transformed into nitrate in the nitrification chain [*Gisi et al.*, 1997]:

$$2NH_4^+ + 3O_2 \rightarrow 2NO_2^- + 2H_2O + 4H^+ \qquad \text{Equation 3}$$

$$2NO_2^- + O_2 \rightarrow 2NO_3^- \qquad \text{Equation 4}$$

Consequently, when all of the urea introduced into our soil core is transformed to nitrate, 0.87 mol of cations and anions are produced. Also, in soil containing organic carbon, chemoorganoheterotrophic processes usually occur, which produce CO_2. This CO_2 is transformed into carbonic acid in the pore fluid, which dissociates to protons and hydrogen carbonate at circumneutral pH. Parallel to the ion producing processes, there are also losses. Gaseous losses of nitrogen occur during denitrification via N_2 and NO_x (during anaerobic conditions) [*Chien et al.*, 2011; *Gisi et al.*, 1997], which results in a net loss of ions from the soil:

$$2C_{org} + 2NO_3^- \rightarrow 2CO_2 + 2H_2O + N_2 \qquad \text{Equation 5}$$

Also uptake of CO_2 during (chemolithoautotrophic) nitrification may result in a reduction of the CO_2 partial pressure and thus in a loss of ions (protons and hydrogen carbonate) from the pore fluid. In summary, however, it is expected that the production of ions exceed the loss of ions, because the heterotrophic, aerobic processes will most likely dominate.

2.3. Electrical resistivity

The electrical resistivity measurements and data processing procedures used here were explained in detail in *Wehrer and Slater* [2015] and are therefore only summarized here. [*Binley*, 2015] provides a comprehensive review of the electrical resistivity method. Electrical measurements were carried out using a SYSCAL Pro resistivity meter (Iris Instruments, Orleans, France) with two extension boxes to accommodate 144 electrodes. Measurements were acquired with dipole-dipole/nearest neighbor type electrode configurations, with current and potential dipoles moving systematically around the soil core in horizontal and in vertical circles. Each set of measurements consisted of 2100 normal and 2100 reciprocal measurements. One measurement sequence took 7 minutes to acquire, so we assume the effect of temporal blurring is negligible, at least for the measurements analyzed in this study, as they were carried out several days after infiltration (usually one week). Measurement errors were estimated using reciprocal error assessment [*Slater et al.*, 2000]. Measurements with more than 10% reciprocal error were removed from the data set and an error model was calculated for the remaining data according to the procedures described in [*Koestel et al.*, 2008] by establishing a functional relationship between classes of magnitudes of resistances of the measurements and the average reciprocal error of these classes. An example of such an error model is provided in the supplemental material of *Wehrer and Slater* [2015]. A forward model error of 2% was added when inverting reference data sets for the difference inversion.

ERT datasets were inverted using the code R3t (v1.8 [*Binley*, 2013]). R3t requires an external program to set up the finite element mesh. We produced a tetrahedral finite element mesh with 234121 elements using gmsh (v2.5 [*Geuzaine and Remacle*, 2009]). The mesh had a fine resolution at the side walls of the cube (characteristic length of tetrahedral elements 1 cm) and coarse resolution in the center of the cube (characteristic length 2 cm). The data set which served as the reference model for the difference inversion (see below) was inverted by a smoothness constrained objective function,

$$\Phi(\mathbf{p}) = \left\| \mathbf{W_d}(\mathbf{d} - f(\mathbf{p})) \right\|^2 + \alpha \left\| \mathbf{W_m p} \right\|^2 \quad . \qquad \text{Equation 6}$$

Here, $\mathbf{d}$ is the data vector and $f(\mathbf{p})$ is the forward model output vector and $\mathbf{W_d}$ is a matrix of data weights, being the inverse of the measurement standard deviations. The parameter vector $\mathbf{p}$ contains the individual logarithm of the conductivity for all

elements. Thus, the first term of Equation 6 is set up to penalize differences of the theoretical data based on the model from the measured data. The parameter α controls the weight of the second term, which is the regularization term containing the roughness matrix $\mathbf{W_m}$ [*Binley and Kemna*, 2005]. R3t optimizes for α at each iteration using a line search in which α is reduced until a minimum data misfit (above the target misfit) is achieved for that iteration. This typically results in α reducing throughout the process.

Time lapse ERT data were inverted by applying the method of *LaBrecque and Yang* [2001]: here, the data vector of each time lapse data set **d'** is replaced by the sum of the data vector containing the differences of the data set **d'** from a reference data set $\mathbf{d_{ref}}$ and a vector containing the forward model results of the reference data set $f(\mathbf{p_{ref}})$ with $\mathbf{p_{ref}}$ being the parameter set of the reference model:

$$\mathbf{d} = \mathbf{d'} - \mathbf{d_{ref}} + f(\mathbf{p_{ref}}) \qquad \text{Equation 7}$$

The approach minimizes the effect of systematic errors on the differences from the reference model. The data set collected directly after introducing the fertilizer served as reference data set. The data vector **d** is used in an objective function, which regularizes the inversion by penalizing differences from the reference model:

$$\Phi(\mathbf{p}) = \left\| \mathbf{W_d}(\mathbf{d'} - \mathbf{d_{ref}} + f(\mathbf{p_{ref}}) - f(\mathbf{p})) \right\|^2 + \alpha \left\| \mathbf{W_m}(\mathbf{p} - \mathbf{p_{ref}}) \right\|^2 \qquad \text{Equation 8}$$

To take error propagation into account, individual errors for the difference measurements were calculated as,

$$\varepsilon_{m,i} = \sqrt{\varepsilon_{recip,ref}^2 + \varepsilon_{recip,i}^2}\,, \qquad \text{Equation 9}$$

where $\varepsilon_{m,i}$ is the individual error of the difference measurement, $\varepsilon_{recip,ref}$ is the reciprocal error of the reference data set and $\varepsilon_{recip,i}$ is the reciprocal error of the measurement. Eq. 9, which is valid for uncorrelated errors of the two measurement sets, was used here, because correlated errors in the two data sets should cancel out by the difference inversion. Information on the sensitivity distribution in the soil core as well as the depth of investigation [*Oldenburg and Li*, 1999] can be found in *Wehrer and Slater* [2015].

For comparison of ERT data with pore fluid or seepage water conductivities we used the following petrophysical relationship [*Breede et al.*, 2011; *Schmutz et al.*, 2010; *Ulrich and Slater*, 2004; *Vinegar and Waxman*, 1984]:

$$\sigma = \frac{1}{F} S_w^n \left[\sigma_w + \frac{\sigma_s}{S_w} \right] ,$$

where [*Archie*, 1942], Equation 10

$$F = \varphi^{-m}$$ Equation 11

Here, σ (S m^{-1}) is the bulk electrical conductivity derived from inverted ERT data, S_w is saturation, F is the formation factor (-), n is Archie's saturation factor (-), σ_w (S m^{-1}) is the pore fluid conductivity and σ_s (S m^{-1}) represents the surface conductivity originating from the electrical double layer forming around charged minerals. Porosity is denoted by φ and m is Archie's cementation factor.

Pore fluid conductivities were estimated from bulk conductivities of every voxel of the finite element mesh of the resistivity model using the average petrophysical parameters derived by *Grunat et al.* [2013] (m = 2.1, n = 1.5, σ_s = 0.008 S m^{-1} φ=0.38 , Equations 10 &11) with undisturbed A-horizon material of the same soil. The water content of every voxel was estimated using a depth dependent polynomial function fitted to the steady state water contents of the three water content probes,

$$\theta(z) = -0.39z^2 + 0.34z + 0.22 .$$ Equation 12

This function incorporates the effect of the vertical gradient of water content into account, resulting from the lower boundary condition. We used the average water content of each probe one week after finalization of each infiltration to set up Eq. 12. As shown in section 3.1, the system returns to steady state water content within one week.

2.5. Spatial moment analysis

The pore fluid conductivity σ_w is related to the equivalent concentration C^{eq} of a charged species via [*Barthel*, 1968]:

$$\sigma_w = \Lambda_c(C^{eq}, \Lambda_0, a, \varepsilon_r, \eta, T) C^{eq}$$ Equation 13

Here, Λ_c is the equivalent molar conductivity (S m^2 mol^{-1}), Λ_0 is the limiting equivalent molar conductivity (S m^2 mol^{-1}) for $C^{eq} \rightarrow 0$, a is the ionic radius (m), ε_r is the relative dielectric constant, η is the viscosity (kg m^{-1} s^{-1}) and T is the temperature (K) of the solution. In order to test a potential estimation of the molar amount of ions and nitrate concentrations from ERT derived bulk conductivities, we established two relationships between the conductivity of the pore fluid solution and ion concentrations. These were based on calculations of the conductivity of two solution types at different total concentrations using PHREEQC Interactive (V 3.3.5 [*Charlton et al.*, 1997]). The first solution type was composed of the reaction products formulated in Equations 2 to 4 plus the input concentration of $CaCl_2$ and the second solution type according to the composition of the seepage water (Table 2; see also results section 3.2). We assume that any solution occurring in the soil core can be thought of as a mixture of these limiting cases. The linearity of the relationships between concentrations and electrical conductivity was tested by simulating additional solutions with the same type as those shown in Table 2 but with intermediate concentrations and fitting a linear regression.

For the case that the relationship in Equation 13 is linear and time- and space-invariant, the changes in fluid conductivity compositions during our experiment could directly be used to track changes of the molar amount of ions. Thus, the zeroth spatial moment for changes in pore fluid conductivity $m_0^{s,c}$ (S m²), based on ERT data, was calculated to derive a measure of changes of the molar amount of ions in the soil core (after *French et al.* [2002]):

$$m_0^{s,c}(t) = \int_0^Z \int_0^Y \int_0^X \theta(x,y,z,t)\Delta\sigma_w(x,y,z,t)dxdydz \qquad \text{Equation 14}$$

Here, x, y and z are the spatial coordinates (m), X, Y and Z the dimensions of the soil core (m), and θ the water content (-). Changes in pore fluid conductivity $\Delta\sigma_w$ are calculated as the pore fluid conductivity at an arbitrary time step versus the initial time step. Thus, the course of $m_0^{s,c}$ over time, calculated with Equation 14, reflects the changes of molar amounts of ions in the soil core from the start of the experiment onwards. The integrals in Equation 14 were approximated by multiplying $\Delta\sigma_w$ of every voxel with its volume and summing up all voxels.

Changes of the molar amount of ions in this soil may occur by import *im* across the upper boundary, export *ex* across the lower boundary or (positive or negative) production *pr* inside the core. Thus, the mass balance allows to derive the amount of ions produced in the soil:

$$\Delta s = im + pr - ex \qquad \text{Equation 15}$$

Here, Δs is the change in storage since start of the experiment. Again, under the assumption of a linear, time- and space invariant relationship according to Equation 13, Equation 15 also holds for pore fluid conductivities. After transforming Δs from molar amounts of ions into pore fluid conductivities it is equal to $\Delta m_0^{s,c}$. Import *im* can then be estimated by calculating the product of input fluid conductivities and input volume and export *ex* by:

$$ex = \int_0^{tc}\int_0^{A} q(t)\cdot\sigma_w(t)dAdt \approx \sum_{j=0}^{j=J}\sum_{i=1}^{i=I}\left[\left(0.5\left(\sigma_{w,i,j}+\sigma_{w,i,j-1}\right)\right)\cdot V_{d,i,j}\cdot A_i\right] \qquad \text{Equation 16}$$

Here, A is the area of the seepage face (m²), *tc* is the truncation time (s) (i.e. the cut-off time of the BTC, *Luo et al.* [2006]), q is the specific discharge (m s^{-1}), J is the total number of time steps, I the total number of voxels with one area of the tetrahedral element in the area of the seepage face, V_d is the drained volume during time step j (m³). Fluid conductivities were again derived from bulk conductivities using the petrophysical function of *Grunat et al.* [2013] and the saturation indicated by the water content probe at 46 cm depth. The export calculated from ERT data was compared to the export calculated by summing up the product of seepage water conductivities and volumes of all seepage water samples during each time step.

2.6. Temporal moment analysis of breakthrough curves of nitrate, seepage water conductivity and ERT derived conductivity

Local BTCs (the term "local" refers to the scale of one compartment of the MCS) of nitrate, seepage water conductivity and conductivity derived by ERT were compared by analyzing shape measures [*Koestel et al.*, 2011; *Wehrer and Slater*, 2015]. ERT estimated conductivities reflect resident concentrations of ions in pore fluids, which can result in deviations from measurement techniques based on flux averaged concentrations under certain conditions [*Singha et al.*, 2007]. A seepage water sample collects a certain volume of pore fluid and an average concentration or

seepage water conductivity is derived from the chemical analysis (flux averaged measurement). To compare both measurement types, it makes sense to compare the bulk conductivity (observed by ERT) of the volume of soil, containing the pore fluid, which is collected as a seepage water sample, to the electrical conductivity of the seepage water sample.

The volume of soil containing the pore fluid, which emerges as seepage water, was estimated from the horizontal dimensions of a single compartment of the MCS and the height of the soil column containing the amount of pore fluid exchanged during an average infiltration event. This height was estimated as 3.50 cm, considering a water filled porosity of 0.38 [*Grunat et al.*, 2013] and drainage of 1.33 cm^3/cm^2, resulting from an average infiltration event. Due to the smoothing during ERT inversion, an approximate average height of 3.5 cm is considered sufficient for the analysis of local conductivities. A local conductivity value was derived from inverted electrical resistivity tomograms by extracting the median conductivity from this volume of soil. We used the median instead of the average as it is more robust against extreme values. ERT bulk conductivities were transformed into fluid conductivities using the saturation indicated by the water content probe at 46 cm depth and the petrophysical function derived by *Grunat et al.* [2013].

The normalized first temporal moment and normalized second central temporal moment, μ_1' (T) and μ_2' (T^2), of a BTC are the mean travel time and its variance and directly related to the mean velocity and apparent dispersivity, respectively [*Koestel et al.*, 2011; *Luo et al.*, 2006]. Reconstruction of the transfer function between input concentration and output concentration allows an estimation of these transport model parameters with minimized influence of noisy data and truncation of the BTC [*Luo et al.*, 2006]. However, in our case the input function is unknown and thus the transfer function can most likely not be reconstructed. Therefore, we chose to estimate the moments directly from discrete measurements of the output concentrations of the truncated breakthrough-curves. Thus, the moment calculation is subject to data error and a systematic error due to truncation. Since we intend a comparison of shapes of breakthrough curves and not an estimation of transport parameters, this procedure is considered appropriate despite the errors involved. However, we found that skewness is particularly sensitive to truncation and abstained from evaluating it. Also, it is important that the compared BTCs are truncated at the same time to avoid a systematic difference. Likewise, it is important that the time steps are fairly

equidistant to avoid biased moments due to over proportional higher weighting of area sections of the BTCs with longer time intervals. For the same reason, we averaged the more finely resolved conductivity measurements to have an equal resolution as the nitrate measurements. For the same reason, missing values for individual samples were linearly interpolated between the previous and the following samples. The normalized moments were calculated as [*Koestel et al.*, 2011; *Luo et al.*, 2006]:

$$\mu_1' = \frac{m_1}{m_0} = \frac{\int_0^{tc} t \cdot C(L,t)dt}{\int_0^{tc} C(L,t)dt} \approx \frac{\sum_{i=1}^{i=k} t_i \cdot \left[\left(0.5\left(C_i + C_{i-1}\right) - C_{\min}\right) \cdot \left(t_i - t_{i-1}\right)\right]}{\sum_{i=1}^{i=k} \left(0.5\left(C_i + C_{i-1}\right) - C_{\min}\right) \cdot \left(t_i - t_{i-1}\right)} \qquad \text{Equation 17}$$

$$\mu_2' = \frac{m_2}{m_0} - \mu_1'^2 = \frac{\int_0^{tc} t^2 \cdot C(L,t)dt}{\int_0^{tc} C(L,t)dt} - \mu_1'^2 \approx \frac{\sum_{i=1}^{i=k} t_i^2 \cdot \left[\left(0.5\left(C_i + C_{i-1}\right) - C_{\min}\right) \cdot \left(t_i - t_{i-1}\right)\right]}{\sum_{i=1}^{i=k} \left(0.5\left(C_i + C_{i-1}\right) - C_{\min}\right) \cdot \left(t_i - t_{i-1}\right)} - \mu_1'^2$$

Equation 18

Here, m_0 (s) is the zeroth temporal moment, m_1 (s²) is the first temporal moment, m_2 (s³) is the second temporal moment, t is time (s) since start of the experiment, tc is the truncation time (s), L is the travel distance (m). Index i denotes the time steps with measurements, k is the number of time steps and C is either (1) concentrations of nitrate in the MCS outflow (kg m^{-3}), (2) seepage water conductivity in the MCS outflow (S m^{-1}), or (3) conductivity derived from ERT directly above the MCS. The minimum measured value of each breakthrough curve C_{min} was used for baseline correction. The baseline of seepage water conductivity and nitrate is different because a constant nitrate-free input conductivity is supplied with each infiltration and further sources of ions, which do not release nitrate, are in the soil. Thus, for a comparison of the BTCs it is reasonable to consider only the baseline corrected part. The exact baseline function for conductivity and nitrate is unknown, but we assume that the error introduced by assuming a constant baseline is minor due to the relative height of the maximum of the BTCs compared to C_{min}. Missing values in BTCs at individual time steps were interpolated linearly for the calculation of the moments.

In this analysis, the BTCs were not referenced to the real time axis but to the amount of cumulative drainage per unit area (m^3 m^{-2}). This has an effect similar to the non-

459 dimensionalization of the time axis, which is derived by referring the BTC to the
460 number of exchanged pore volumes [*Toride et al.*, 1999; *Wehrer and Slater*, 2015].
461 As a result, the moments μ_1' and μ_2' will have the units of (m) and (m²) subsequently.
462 Nitrate and seepage water conductivity measurements were attributed to half of the
463 drainage amount occurring during one infiltration and the ERT measurements were
464 attributed to the amount of drainage occurring until this measurement.

3. Results

3.1. Evolution of water content and tension over time

Figure 2 shows the changes of water contents and tensions during the 22 infiltration events throughout the experiment. Fertilizer was added into the soil on 18th Sept. 2013. Coincident with the increase of water contents, tensions decrease during infiltration events, with the probes nearest to the surface showing the most pronounced response. Water contents and tensions return to steady state conditions within about one week after each infiltration. During 9th Oct. 2013 and 18th Dec. 2013 the suction at the lower boundary was increased to 100 cm, resulting in higher tensions and lower water contents. Before addition of the fertilizer, 24 infiltrations were carried out to observe the breakthrough of a conservative tracer. Water contents and tensions during this period are published in *Wehrer and Slater* [2015] (their Figure 3).

Figure 2

3.2. Breakthrough of major ions and electrical conductivity observed in the MCS outflow

For an evaluation of the breakthrough behavior on the scale of the entire lysimeter, all samples collected from the start of one infiltration to the start of the next infiltration were combined and analyzed for the major cations and anions after the analyses for individual compartments were completed. Figure 3 shows the changes of concentrations of NO_3^-, Ca^{2+}, Mg^{2+}, and electrical conductivity in the combined samples versus cumulative discharge (i.e. time). Not shown are the concentrations of H_3O^+, Cl^-, Na^+ and K^+. Oxonium was present in very low amounts from $3*10^{-5}$ to $4*10^{-3}$ mmol/l (i.e. pH 5.4 to 7.5). Cl^-, Na^+ and K^+ exhibited relatively constant outflow concentrations around mean values of 4.4 meq/l, 0.52 meq/l and 0.45 meq/l, respectively. Nitrate is the dominant anion during the breakthrough and mainly balanced by calcium and magnesium. Nitrate was already present before adding the fertilizer and is therefore leached starting from the beginning of the experiment. Magnesium was presumably present in the soil before extraction of the core and calcium is repeatedly added with the infiltration solution. The nitrate already present

497 resulted from earlier fertilizer applications, which were carried out before the soil core
498 was extracted in the field and transported to the laboratory. The electrical conductivity
499 of the soil solution rises from 0.86 mS/cm to 1.86 mS/cm during the breakthrough of
500 NO_3^-, Ca^{2+}, Mg^{2+}. A complete mass balance for nitrogen is not possible due to the
501 unknown change of storage in the soil, unknown gaseous losses and the fact that not
502 all aqueous samples were analyzed for nitrate. A total of 4.0 g nitrogen was added to
503 the soil as fertilizer and approximately 4.8 g nitrogen was exported as nitrate during
504 the experiment.

505

506 Figure 3

507

508 *3.3. Qualitative evaluation of time lapse ERT during nitrate production and transport*

509 Figure 4 shows the development of the bulk resistivity in the soil core since addition
510 of the fertilizer to the soil core. Displayed are resistivities below a threshold of $10^{2.05}$
511 Ωm (112 Ωm), which is a little lower than the minimum resistivity at the start of the
512 experiment in the region of the fertilizer application (118 Ωm). The ERT
513 measurements for the tomograms were carried out at near constant water contents
514 after equilibration of the soil water states following each infiltration (indicated by
515 green broken lines in Figure 2). The tomograms primarily reflect changes of pore fluid
516 conductivity, as can be demonstrated by estimating relative changes in water content
517 and σ_w over the experiment duration. The decrease of water content between the
518 ERT measurement on the 18th Sep 2013 and on the 18th Dec 2013 due to the
519 changes of the lower boundary is the largest in between any ERT measurement and
520 the reference date. It amounts to 5% at the bottom (it is largest at the bottom, where
521 the boundary condition was changed). Thus, the factor S^n in the petrophysical
522 function (Eq. 10) changes by 22% (assuming n=1.51 and porosity=0.38), while at the
523 same time the factor σ_w changes by - on average - 120% at the lower boundary due
524 to the breakthrough of the fertilizer (note that this does not represent the largest σ_w
525 change in the entire core as it is prior to the peak breakthrough at the boundary).

526 At day 0 the bands of fertilizer application are indicated by two parallel red lines. The
527 upper part of the soil core has resistivities larger than the threshold of 110 Ωm, a
528 region of low resistivity is visible at the bottom of the core. This region most likely

originates from the tailing of a high pore fluid conductivity plume from a previous experiment, published in *Wehrer and Slater* [2015], or from the wetter conditions near the bottom of the core. The threshold of 112 Ωm was chosen because it seems to show the shape of the plume of low resistivity expanding in the region of fertilizer application and propagating through the soil core. Initially, two separate plumes develop around the bands. This separation is only visible near the outside of the core, were the sensitivity of the ERT model to the data is greatest. Towards the inside of the core, the plumes merge (not shown). The area of reduced resistivity grows and propagates downwards through the soil core during the consecutive infiltrations until it reaches the lower boundary and is washed out. Resistivity in this region subsequently increases due to progressive dilution. Thus, the general spatio-temporal behavior of nitrate production and leaching is observable by ERT.

Figure 4

3.4. *Spatial moment analysis of ERT results*

In the following paragraphs, we explore the ability of ERT to characterize the source zone in more detail. The relationship between pore fluid electrical conductivity and concentration of target ions is essential for the interpretation of conductivities derived by ERT. Our result calculated with PHREEQC interactive (Table 2) showed that this relationship is linear for both types of solutions (R^2>0.999), but the slope of the regression is about 6-fold larger for the second solution type (=products of the nitrification reaction; see section 2.5) compared to first solution type (=seepage water composition; see section 2.5). This is due to the much larger molar conductivity of H^+ compared to other ions and means that much lower molar concentrations of ions of the second solution type will result in the same pore fluid electrical conductivity as the first solution type. The second solution type has a very acidic pH of smaller than 1 to around 2.

Figure 5 shows the results of the spatial moment analysis. The change in storage Δs (Equation 14); note that "change" always means the change towards the initial conditions, i.e. day 0) shows an initial rise of the storage until day 35 (Figure 5a), then effectively hardly any change until day 125, a rapid decline until day 166,

followed by constant storage until the end of the experiment at a higher level than the start of the experiment. Parts of this behavior can be explained by import and export of ions. If no production occurs, changes in storage would equal the difference import-export. This difference indicates a slow decline until day 125, then a rapid decline until day 166, followed by a slower decline (Figure 5a). The rapid decline after day 125 perfectly mirrors the rapid decline of Δs, thus this part of Δs can be explained by the difference of import-export. However, the initial rise in storage until day 35 is not due to import and can only be explained by production of ions. This rate of production diminishes after day 35 but balances the export, thus, between day 35 and day 125 and after day 166 no changes in storage are observed.

Figure 5b shows an estimation of the change in storage and the export of the molar amounts of nitrate based on ERT data compared to the measured amounts in the seepage water. The ERT derived pore fluid conductivity σ_w was transformed into nitrate concentration C_{NO3} using the PHREEQC derived regression for the first solution type (C_{NO3} (mol/m³)= 88.85 mol/(S m²)*σ_w - 3.51 mol/m³). The export agrees quite well, except for the final part of the curve.

For validation of the ERT estimates, Figure 5a also shows a comparison of the export of ions estimated by ERT and estimated from measurements of seepage water conductivity. Both agree fairly well, considering that pore fluid conductivity estimated from ERT data are based on an independently derived petrophysical function applied to inverted ERT data.

Figure 5

3.5. Validation of ERT results with MCS outflow data

For a validation of the ERT results we aim for a quantitative comparison of spatially resolved breakthroughs observed by ERT and by nitrate analysis in seepage water samples of the MCS. The breakthrough characteristics of seepage water conductivity are also shown to provide information on the origin of the deviations of ERT BTCs from nitrate BTC characteristics. Figure 6 shows the breakthrough-curves of nitrate, seepage water conductivity and conductivity derived from ERT surveys at two compartments. Compartment B5 (Figure 6a) showed high flow (on average 6.1 % of

593 the total outflow each infiltration) and compartment E4 (Figure 6b) showed low flow
594 (on average 0.6% of the total outflow each infiltration). The BTCs agree well in
595 qualitative terms. They show initially non-zero values and a pronounced peak with an
596 asymmetric shape with a rapid increase and a slow decline. Deviations due to
597 analytical noise and systematic shifts of the BTCs can partly be observed. Most
598 pronounced is the shift of the ERT BTC to earlier times (i.e. cumulative discharge) in
599 compartment E4. The BTCs of seepage water conductivity and ERT seem to have a
600 reduced peak height to tailing ratio compared to the nitrate peak.

601

602 Figure 6

603

604 ERT derived conductivity BTCs were validated by comparison of their shape
605 measures with the respective shape measures of nitrate BTCs and seepage water
606 conductivity BTCs in samples of the draining compartments of the multicompartment
607 sampler. Figure 7 shows the respective scatter plots and Table 3 gives the
608 correlation coefficients. The normalized first central moment μ_1' is highly correlated
609 between the three variables and close to the 1:1 line. There appears to be a slight
610 systematic deviation to larger μ_1' of seepage water conductivity and ERT compared
611 to nitrate. The correlation of μ_2' is much less pronounced, yet still significant. The
612 ERT derived μ_2' shows a systematic shift to larger values, while μ_2' of seepage water
613 conductivity is scattered around the 1:1 line. Significant correlations were derived for
614 the maximum of the BTCs and the area under the BTCs (Figure 7 c) and d)). In both
615 cases, the relationship between ERT and nitrate has a larger slope than the
616 relationship between seepage water conductivity and nitrate.

617

618 Figure 7

619

620 With respect to characterization of nitrate transport, it is of interest to consider how
621 the properties of the source function are reflected in the breakthrough and whether
622 these properties are reflected in the ERT measurements. For this purpose, a
623 comparison of nitrate breakthrough of this fertilizer experiment and bromide
624 breakthrough of a previous tracer experiment (published in *Wehrer and Slater* [2015])

was performed. Figure 8 shows the difference of the nitrate BTC to the bromide BTC for the example of compartment B5. The BTCs from the tracer experiment are transfer function fits to experimental data. It is obvious that the peak of the nitrate BTC is broader and a longer tailing can be observed. These shape characteristics are also observable in the ERT data for compartment B5. Compared to bromide, area and maximum of the nitrate BTCs are much larger due to the higher mass of nitrogen added to the system in the fertilizer experiment (note the different scaling of the y-axes).

Figure 8

We now examine whether the change in shape characteristics between bromide and nitrate BTCs are observable for other compartments. The broadened peak and the longer tailing of the nitrate BTC results in a delay of the mean arrival time, i.e. a larger normalized first central moment μ_1' and an increase of variance, i.e. a larger μ_2'. Figure 9 shows the changes in normalized first moments between BTCs of the fertilizer versus the conservative tracer experiment published in *Wehrer and Slater* [2015] depending on compartment location. As expected from the example of compartment B5 presented in Figure 8, there is a systematic shift to larger mean travel times in the fertilizer experiment. Notably, the two rows of compartments on the edge of the plate (row 1 and row 6) parallel to the fertilizer bands show an even greater shift to larger μ_1' than the other rows. This effect appears somewhat more pronounced in the ERT data. Nevertheless, the mean travel times of the fertilizer and tracer experiment are highly correlated, which is in opposition to the variances (Table 1). The variances of the fertilizer experiment are shifted to larger values (Figure 10) but they are not correlated between the two experiments (Table 3).

Figure 9

Figure 10

655 Figure 11 examines whether the differences observed in mean travel times of nitrate
656 and bromide are preserved in the ERT data. Here, the differences $\Delta\mu_1'$ between
657 fertilizer and tracer experiment of ERT derived BTCs and seepage water conductivity
658 BTCs are plotted versus the respective differences of BTCs derived from analyses of
659 nitrate and bromide in seepage water samples of the MCS. The respective
660 correlation coefficients are shown in Table 3. The differences are well preserved for
661 μ_1' and a significant correlation is observed.

662

663 Figure 11

4. Discussion

According to the processes in the nitrogen cycle, the production of nitrate from urease via ammonia involves the production of protons [*Chien et al.*, 2011; *Gisi et al.*, 1997]. The protons are exchanged against calcium and magnesium at sorption sites. Calcium is repeatedly introduced with the input solution and magnesium most likely was present in the soil from the beginning of the experiments. Consequently, the breakthrough of nitrate in our experiment is counterbalanced by these cations and not by H_3O^+ (Figure 3). Only a delayed and (amount-wise) insignificant breakthrough of oxonium occurs, indicating an almost complete buffering of the pH decrease. Considering the estimation of input and output masses, it can be assumed that most of the fertilizer nitrogen was exported from the soil as nitrate. Additional N, probably from degradation of soil organic matter, was exported in the form of nitrate, as the output of nitrate-N was larger than the N input via fertilizer. In the field, plants would take up a large part of the nitrogen. Also, the input of easily degradable organic C from root exudates and plant residues would probably enhance denitrification. Thus, the high concentrations of nitrate in the seepage water of our soil core represent a worst case scenario with respect to environmental impact.

The response of the electrical conductivity in the soil core recovered by the time lapse resistivity tomograms at fairly constant water contents (Figure 4) is mainly governed by the production and leaching of nitrate and the mobilized cations. The characterization of spatially heterogeneous and time variant sources of ions and their subsequent transport through the unsaturated zone is limited by the smoothing regularization of the inversion. *Koestel et al.* [2009a] showed that isolated spots of electrical conductivity contrasts, e.g. between two preferential flow paths, are not well recovered. In our results, the conductivity peaks at the location of the fertilizer bands are certainly smaller than in reality and conductivity contrasts in the region between the two fertilizer bands are concealed by the large conductivity increase at the fertilizer bands. Nevertheless, the development of electrical conductivity over time in the source zone (Figure 5) is physically meaningful: The difference between import and export agrees well with the magnitude of the strong decrease in storage during days 125 to 166. This strong decrease in storage is due to the peak of the breakthrough of nitrate and cations being exported via the lower boundary. Also, the characteristics of the production curve with a rapid initial increase and a slower subsequent increase agree with the general characteristics of a slow release

698 fertilizer. In field trials, about 80% of the nitrogen was released from the ESN 44-0-0
699 within 6 weeks in the soil, the remaining 20% was released in another 6 weeks
700 [Sanwald and Wiseman, 2008].

701 For a quantitative interpretation of bulk conductivities with respect to fluid
702 conductivities and potentially concentrations of a target ion, several assumptions
703 about the relationship between these variables must be made. This requires first a
704 parameterization of Eq. 10. In our case, we only had a single petrophysical function
705 [*Grunat et al.*, 2013]. This petrophysical function is a large source of uncertainty.
706 Estimating the export (Figure 5a and b) using the parameters determined for the two
707 individual columns, m=2.24/n=1.03 and m=1.88/n=1.98, as published by *Grunat et al.*
708 [2013] instead of the averaged petrophysical parameters, would result in 7% larger
709 and minor export estimates, respectively. Certainly, two columns will not cover the
710 entire range of variability of the petrophysical function in the core, so the uncertainty
711 is likely to be larger. The establishment of locally heterogeneous petrophysical
712 functions remains a challenging problem in hydrogeophysics [*Dafflon and Barrash*,
713 2012; *Moysey et al.*, 2005].

714 The use of the petrophysical function also requires an estimation of the water
715 content. We were able to delineate an equation to take account of the vertical
716 variability of soil water content in the column (Eq. 12). However, we are not able to
717 take horizontal variability of water content into account. Such horizontal variability
718 could add bias to the analysis of spatial moments. However, since we look at
719 conductivity differences at fairly constant water contents, this bias is minimized (given
720 we can assume that the water content at each location is repeatedly going back to
721 the water content at the reference date).

722 If we aim for an estimation of solute concentrations from bulk conductivities not only
723 the petrophysical function is required, but also a relationship between the fluid
724 conductivity and the solute concentration (Eq. 13). We assume that the pore fluid in
725 the region of fertilizer application is similar in composition to the seepage water and
726 not the composition resulting from the nitrification reaction. There are several
727 arguments supporting this assumption. Ion exchange reactions are relatively rapid,
728 so protons will be exchanged against magnesium and calcium without delay, if
729 available. Since the pH of the soil solution is near neutral and calcium is continuously
730 provided with the input solution, it can be expected that ion exchange sites are

saturated with base cations. Furthermore, at extremely low pH, the microbial nitrification will be limited, so without continuous buffering, only limited ion production would occur. In addition, the strong increase in storage until day 35 due to production has about the same magnitude as the decrease during days 125 to 166. This supports the argument that the relationship between ion concentration and pore fluid conductivity is the same, because the same amount of ions produced needs to be exported. The magnitude of error related to the relationship between solute concentration and fluid conductivity is likely to be on the order of a few percent and adds to the error resulting from the application of a homogeneous petrophysical function. Thus, the nitrate export estimated by ERT (Figure 5b) indicates that we derived a realistic estimate, but the good fit to the actual nitrate export should not be interpreted as generally valid.

The analyses of shape measures of local breakthrough curves show that local differences in the normalized first moment can be recovered quantitatively with ERT (Figure 7a). The reason for the slight systematic shift of μ_1' between seepage water conductivity and ERT compared to nitrate is due to the moments being calculated for truncated asymmetric BTCs. For seepage water conductivity and ERT μ_1' is shifted to higher values because the tailing receives a larger weight in their BTCs (i.e. the peak appears lower compared to the tail than in the nitrate BTCs) owing to the nonlinear relationship between activity and concentration of nitrate. In the case of ERT further error is introduced by the smoothing regularization. Additional error comes from the different temporal resolution of seepage water conductivity and nitrate and also from the need to attribute the measurements to different points of the time axis (i.e. attributing nitrate and seepage water conductivity measurements to half of the drainage amount occurring during one infiltration and the ERT measurements to the amount of drainage occurring until this measurement). Also the of type of bias *Singha et al.* [2011] observed in estimates of temporal moments of a NaCl breakthrough by ERT in the presence of ion exchange processes needs consideration. Extrapolated to our case, this effect should result in differences between the production related change of storage and export related change of storage, which is also on the order of a few percent.

In contrast to the normalized first moment μ_1', local differences in the variance μ_2' are barely resolvable by ERT and also the mean of the variances is overestimated

764 (Figure 7b). On the contrary, the mean of variances of seepage water conductivity
765 breakthroughs agrees fairly well with nitrate. This observation apparently contradicts
766 the results of *Wehrer and Slater* [2015], where the local dispersivities of the bromide
767 breakthrough observed by ERT and seepage water conductivity were distributed
768 across similar intervals. The reason is that in the former experiment, the tracer peak
769 conductivity was only slightly larger than the background conductivity, while in the
770 fertilizer experiment, the nitrate induced conductivity peak is much larger. This results
771 in a stronger influence of smoothing during the inversion of ERT data and in larger
772 variances of breakthrough curves derived from ERT compared to seepage water
773 conductivity. Nevertheless, the lower background and higher peak maximum of the
774 nitrate breakthrough results in a significant relationship between μ_2' of ERT and
775 seepage water conductivity and nitrate. Thus, when using ERT to characterize tracer
776 transport, there is a tradeoff between selecting either a tracer with a relatively low
777 conductivity to minimize smoothing artifacts on the variances of local BTCs and
778 recover the mean of variances versus selecting a tracer with a high conductivity to
779 maximize the observed peak and potentially recover local differences of variances
780 and also peak areas, as discussed subsequently. Fortunately, the recovery of the
781 mean travel time of BTCs (μ_1') by ERT is relatively little influenced by smoothing
782 artifacts and size of the tracer peak above the background conductivity.

783 Local differences in peak maximum and area can also be resolved (Figure 7 c & d).
784 The petrophysical function [Grunat et al., 2013] likely transformed part of the ERT
785 derived BTCs correctly into seepage water conductivity BTCs. However, some
786 locations would have required different petrophysical functions, resulting in the visible
787 differences of the relationships between nitrate and seepage water on the one hand
788 and ERT and nitrate on the other hand (Figure 7c & d). Apparently, the lack of a
789 locally heterogeneous petrophysical function introduces a larger error in the
790 estimation of peak size than in the estimation of temporal moments, i.e. location of
791 the peak with respect to the time axis. Nevertheless, the information derived by ERT
792 on the heterogeneous distribution of different maxima and areas of the peak could
793 emerge as helpful in fate modeling of nitrogen in agricultural soils. The ERT
794 information sets additional constraints for such models, because it delimits the spatial
795 relationships of local peak maxima and areas of breakthrough curves in a soil core.

796 It is highly encouraging that areas under the BTCs derived by ERT and by nitrate
797 analysis are correlated; this was not the case for the bromide BTCs in the experiment

published by *Wehrer and Slater* [2015]. This is attributed to the much larger peak of nitrate induced conductivity in the fertilizer experiment, emphasizing the advantage of a larger conductivity contrast with the background fluid. In contrast, the correlation of the maximum of the BTCs is little influenced by peak size. To estimate mass flux, which is essential with respect to management scenarios, it is necessary to know – firstly – the area of a breakthrough curve and – secondly – the specific discharge. Information on the specific discharge is carried by the peak timing of a conservative tracer under certain conditions (see discussion in *Wehrer and Slater* [2015] and *Vanderborght and Vereecken* [2001]). Since time lapse ERT delivers spatially resolved information on both factors, we see a potential application of ERT for fertilization monitoring and management, which goes beyond the capabilities of traditional methods.

The bromide tracer was applied uniformly to the top of the core and spatial differences of moments of different compartments are only attributed to the occurrence of heterogeneous flow paths in the soil core [*Wehrer and Slater*, 2015]. In contrast, the fertilizer was added in two parallel bands and released urea over a period of several weeks. This urea was then converted to nitrate in a rate dependent reaction. Thus, differences observed in the local breakthrough curves of bromide and nitrate result in systematically larger means and variances of travel times of nitrate BTCs (Figures 8, 9 and 10). The high correlation of mean travel times between the two experiments implies that the principal influence of preferential flow pathways was preserved, irrespective of the different application modes of the two compounds analyzed. Thus, despite the retarded release and production of nitrate, on average all molecules experience the same rapid or slow flow paths as bromide molecules. This suggests that mixing in the top layer is relatively efficient and divergence of flow paths must occur deeper down. This result shows that the non-invasive continuous monitoring ERT data provides unique information for the characterization of the influence of preferential flow processes on reactive species. The assumption of a divergence of flow paths below the top layer corroborates the assumption made by *Wehrer and Slater* [2015] that the preferential flow in this soil core is related to the plow pan.

Only minor systematic spatial differences in breakthrough behavior of nitrate and bromide are observed, reflected in the larger mean travel times of rows 1 and 6 (Figure 9). This is most probably a result of the larger distance of these two rows

832 (relative to the other rows) from the location of fertilizer addition and therefore a
833 longer travel time of the nitrate pulse. Although it is valuable that even such relatively
834 small effects of lateral mass transport are still recovered by ERT, it must be noted
835 that the difference of rows 1 and 6 relative to the other rows is more pronounced in
836 the ERT data, pointing to the influence of additional boundary effects. Also, individual
837 compartments sometimes show distinctly different results for ERT and nitrate BTCs.
838 Nevertheless, spatial variability in the delay of the nitrate peak relative to the bromide
839 peak can be observed with ERT (Figure 11).

840 In contrast to the mean travel time, the variances of the two experiments are not
841 correlated. This is a consequence of the different processes affecting the variances in
842 the two experiments. In the tracer experiment, the variance is influenced by
843 dispersivity, including the potential exchange between mobile and immobile water. In
844 the fertilizer experiment, the variance is additionally influenced by the duration of the
845 release of nitrogen and the transformation rate of nitrate. The lack of correlation
846 means that, in contrast to the mean travel time, the variance of nitrate travel times is
847 largely determined by the variance induced by the release and production process
848 and less by the dispersion processes along the travel path as in the case for bromide.

849 The field-scale application of ERT for quantifying spatially heterogeneous production
850 and transport of nitrate is subject to some additional limitations relative to what has
851 been demonstrated here. The peak of the conductivity breakthrough will be much
852 smaller due to the consumption of nitrogen by crops. However, literature shows that
853 10-20% of applied nitrogen is also leached under field conditions [*Van Breemen et*
854 *al.*, 2002; *Velthof et al.*, 2014]. Additional interference comes from other ions and
855 reactions occurring in agricultural soils. Evapotranspiration will reduce the velocity of
856 the downward propagation of the plume, resulting in relatively enhanced dispersion
857 and in enhanced background conductivity. Dissolution of soluble salts and intense
858 microbial degradation of organic matter would obstruct the nitrate breakthrough as
859 they likewise produce ions. Consequently, ERT should be accompanied by pore fluid-
860 and water content measurements in agricultural soils whenever possible, in order to
861 constrain the effect of other process and obtain (at least spot-wise) groundtruthing.

862 In our experiment, the peak nitrate concentrations and resulting seepage water
863 conductivities were much higher at a smaller background conductivity than in our
864 previous experiment with bromide [*Wehrer and Slater*, 2015]. There, the conditions

865 for a recovery of the breakthrough by ERT were much worse. Peak Br^-
866 concentrations were about 200 mg/l, with a very variable and high fluid conductivity
867 background, because the bromide breakthrough occurred on the elution curve of soil
868 borne nitrate. These conditions probably reflect the lower boundary of a quantitative
869 interpretation of time lapse ERT with respect to effects of heterogeneous transport.

870 The figure of 200 mg/l depends on the characteristics of the background pore fluid
871 and potential additional reactions. Detectability gets better with less background
872 conductivity. An important consideration is the time dependency of additional ion
873 producing or consuming reactions. For example, a worst case for the quantification of
874 a nitrate breakthrough by ERT would be another process producing a peak of other
875 mobile ions around the same magnitude and around the same time of the year when
876 fertilization is carried out. This would impede the estimation of moments related to the
877 nitrate breakthrough. On the other hand, a process producing ions fairly at steady
878 state would interfere less with time lapse ERT. Surface conductivity will only have a
879 limited influence on the estimation of moments, as it is unlikely to exhibit large
880 changes over time. Nitrate peaks due to fertilization will be less diluted and dispersed
881 near to the surface, but the potential to observe the nitrate breakthrough diminishes
882 with depth.

883 The requirement of conducting regularly ERT surveys at constant water contents to
884 receive a tracer breakthrough is probably a critical limitation. Yet, water contents
885 return to field capacity after precipitation and periods of high evapotranspiration (i.e.
886 summer) with very low water contents will at the same time not result in further
887 propagation of a tracer plume [*Lissner et al.*, 2014; *Wehrer et al.*, 2014]. Under the
888 specific experimental conditions, small changes of water content appear to have
889 limited influence on the temporal moments of a tracer breakthrough observed by
890 ERT. In deeper soil horizons the variability of water content will be quite limited
891 [*Wehrer et al.,* 2014]. Another limitation can be the reduced sensitivity of ERT in the
892 field. Certainly, a similar resolution can only be achieved by applying the same
893 distance of electrodes in a vertical array around a soil core of similar size. Even
894 compared to this situation, our laboratory set up has the advantage that due the
895 lysimeter casing, the current dispersion is limited to the soil core. Without the casing,
896 current will also disperse into the soil beyond the boundary electrodes, reducing
897 resolution.

5. Conclusions

We have shown that time-lapse ERT can provide quantitative information on the spatial heterogeneity of nitrate production and transport. The smoothing algorithm during inversion reduces spatial differences in areas, which are concealed by large conductivity increases in the source zone, hampering the recovery of the variances of travel times from breakthrough-curve analysis. Other shape measures of the breakthrough curve, like normalized first moment, maximum and area are highly correlated between measured nitrate and ERT derived BTCs indicating that spatial differences of mean travel times and mass transport are preserved in the ERT data.

Thus, despite the limitations, there remains little doubt that ERT time-lapse data carries information on spatially heterogeneous source zone processes and transport of reactive species. We showed that ERT supports process inference qualitatively and offers opportunities for quantitative exploitation. While the direct interpretation of time lapse ERT data with respect to specific ion concentrations may be limited, ERT data can be used to inform unsaturated flow and transport models, because it can set constraints that cannot be provided by conventional methods. However, it would be advantageous to incorporate data from other sources via joint and coupled inversion techniques [*Finsterle and Kowalsky*, 2008; *Looms et al.*, 2008].

One example, where ERT time lapse data could be helpful is the nitrate leaching component of nitrogen budgets. For agricultural soils, amounts of leaching nitrate are often derived using suction cup samples or soil sampling in combination with simple water balance or bucket models [*Loubet et al.*, 2011; *Skiba et al.*, 2009; *Wyland et al.*, 1996]. This method has very limited opportunities to take spatial heterogeneity into account with a reasonable temporal resolution. Also, nitrogen species transformations and transport are not well represented in laboratory experiments and are difficult to be determined in their entirety in the field, due to the relatively large number of interdependent microbial and plant driven processes. This requires a coordinated set of field tools being able to deliver information on each component of the nitrogen cycle. ERT can contribute to this with a more detailed picture of the production and leaching of nitrate, because ERT is able to monitor these processes directly at the location of the source without disturbing sampling of the microbially-induced processes over the whole period of time.

Inclusion of ERT data into models of nitrogen fate will require strategies to involve the spatially resolved information while taking account of inversion artifacts like smoothing and concealing of local conductivity differences and the uncertainty involved in applying a petrophysical function to interpret bulk conductivities with respect to fluid conductivities.

Acknowledgements

This study was supported by the DFG (WE 4979/1-1). We thank Rebecca Wiseman and Kevin Sanwald form the Cornell University cooperative extension of Suffolk County for financial and field work support and we thank Jin Young Shin, Cheryl Yao and Erika Baldino of the Meadowlands Environmental Research Institute for support with the analytical work. We also thank Rutgers and NJIT students Sherief Saleh, Melissa Belot and Barbara Goldman for help with the experimental work. The data used to produce the results of this paper can be obtained from the corresponding author (markus.wehrer@uni-jena.de).

Literature

Archie, G. E. (1942), The electrical resistivity log as an aid in determining some reservoir characteristics. , *Petroleum Development and Technology, Proc. Amer. Inst. Min. Met. Eng.* , *146*, 54-62.

Bakhsh, A., R. S. Kanwar, and J. L. Baker (2010), N-Application Methods and Precipitation Pattern Effects on Subsurface Drainage Nitrate Losses and Crop Yields, *Water Air Soil Poll.*, *212*, 65-76.

Barthel, J. (1968), Conductance of Electrolyte Solutions, *Angew. Chem.-Int. Edit.*, *7*, 260-&.

Beven, K., and P. Germann (2013), Macropores and water flow in soils revisited, *Water Resour. Res.*, *49*, 3071-3092.

Binley, A. (2013), R3t, version 1.8., edited, Lancaster University, Lancaster, UK.

Binley, A. (2015), Tools and Techniques: Electrical Methods in *Treatise on Geophysics (Second Edition)*, edited by G. Schubert, pp. 233-259, Elsevier, Oxford.

Binley, A., S. HenryPoulter, and B. Shaw (1996), Examination of solute transport in an undisturbed soil column using electrical resistance tomography, *Water Resour. Res.*, *32*, 763-769.

Binley, A., and A. Kemna (2005), DC Resistivity and Induced Polarization Methods, in *Hydrogeophysics*, edited by B. Rubin and S. S. Hubbard, pp. 129-156, Springer.

Bloem, E., J. Vanderborght, and G. H. de Rooij (2008), Leaching surfaces to characterize transport in a heterogeneous aquifer: Comparison between flux concentrations, resident concentrations, and flux concentrations estimated from temporal moment analysis, *Water Resour. Res.*, *44*, W10412.

Blume, H. P., et al. (2010), *Scheffer/Schachtschabel: Lehrbuch der Bodenkunde*, Spektrum Akademischer Verlag, Heidelberg, Germany.

Breede, K., et al. (2011), Joint Measurement Setup for Determining Spectral Induced Polarization and Soil Hydraulic Properties, *Vadose Zone J.*, *10*, 716-726.

Bundt, M., et al. (2001), Preferential flow paths: Biological 'hot spots' in soils, *Soil Biology and Biochemistry*, *33*, 729-738.

Charlton, S. R., C. L. Macklin, and D. L. Parkhurst (1997), PHREEQCI - a graphical user interface for the geochemical computer program PHREEQC, *US Geological Survey Water-Resources Investigations Report*, *9*.

Chien, S. H., M. M. Gearhart, and S. Villagarcia (2011), Comparison of Ammonium Sulfate With Other Nitrogen and Sulfur Fertilizers in Increasing Crop Production and Minimizing Environmental Impact: A Review, *Soil Science*, *176*, 327-335.

Clothier, B. E., S. R. Green, and M. Deurer (2008), Preferential flow and transport in soil: progress and prognosis, *Eur. J. Soil Sci.*, *59*, 2-13.

Dafflon, B., and W. Barrash (2012), Three-dimensional stochastic estimation of porosity distribution: Benefits of using ground-penetrating radar velocity tomograms in simulated-annealing-based or Bayesian sequential simulation approaches, *Water Resour. Res.*, *48*, W05553.

Daily, W., et al. (1992), Electrical-Resistivity Tomography of Vadose Water-Movement, *Water Resour. Res.*, *28*, 1429-1442.

Day-Lewis, F. D., and K. Singha (2008), Geoelectrical inference of mass transfer parameters using temporal moments, *Water Resour. Res.*, *44*.

Dubrovsky, N. M., et al. (2010), *The Quality of Our Nation's Water: Nutrients in the Nation's Streams and Groundwater, 1992-2004*, US Department of the Interior, US Geological Survey.

European Commission (2011), REPORT FROM THE COMMISSION TO THE COUNCIL AND THE EUROPEAN PARLIAMENT on the implementation of Council Directive 91/676/EEC concerning the protection of waters against pollution caused by nitrates from agricultural sources based on Member State reports for the period 2008–2011, Brussels.

Finsterle, S., and M. B. Kowalsky (2008), Joint hydrological-geophysical inversion for soil structure identification, *Vadose Zone J.*, *7*, 287-293.

Flipse, W. J., and F. T. Bonner (1985), Nitrogen-Isotope Ratios of Nitrate in Ground Water Under Fertilized Fields, Long Island, New York, *Groundwater*, *23*, 59-67.

Fluhler, H., W. Durner, and M. Flury (1996), Lateral solute mixing processes - A key for understanding field-scale transport of water and solutes, *Geoderma*, *70*, 165-183.

French, H. K., et al. (2002), Monitoring snowmelt induced unsaturated flow and transport using electrical resistivity tomography, *J. Hydrol.*, *267*, 273-284.

Garre, S., et al. (2010), Comparison of Heterogeneous Transport Processes Observed with Electrical Resistivity Tomography in Two Soils, *Vadose Zone J.*, *9*, 336-349.

Gerke, H. H., P. Germann, and J. Nieber (2010), Preferential and Unstable Flow: From the Pore to the Catchment Scale, *Vadose Zone J.*, *9*, 207-212.

Geuzaine, C., and J.-F. Remacle (2009), Gmsh: A 3-D finite element mesh generator with built-in pre- and post-processing facilities, *International Journal for Numerical Methods in Engineering*, *79*, 1309-1331.

Gisi, U., et al. (1997), *Bodenökologie*, 2nd ed., Georg Thieme Verlag, Stuttgart.

Grunat, D., L. Slater, and M. Wehrer (2013), Complex electrical measurements on an undisturbed soil core: evidence for improved estimation of saturation state from imaginary conductivity, *Vadose Zone J.*, *12*.

Hendrickx, J. M. H., and M. Flury (2001), Uniform and preferential flow mechanisms in the vadose zone, in *Conceptual models of flow and transport in the fractured vadose*

zone, edited by N. Research and Council, pp. 149-187, National Academy Press, Washington, DC.

Irving, J., and K. Singha (2010), Stochastic inversion of tracer test and electrical geophysical data to estimate hydraulic conductivities, *Water Resour. Res.*, *46*.

Koestel, J., et al. (2009a), Imaging Brilliant Blue Stained Soil by Means of Electrical Resistivity Tomography, *Vadose Zone J.*, *8*, 963-975.

Koestel, J., et al. (2008), Quantitative imaging of solute transport in an unsaturated and undisturbed soil monolith with 3-D ERT and TDR, *Water Resour. Res.*, *44*.

Koestel, J., et al. (2009b), Noninvasive 3-D Transport Characterization in a Sandy Soil Using ERT: 2. Transport Process Inference, *Vadose Zone J.*, *8*, 723-734.

Koestel, J., et al. (2009c), Noninvasive 3-D Transport Characterization in a Sandy Soil Using ERT: 1. Investigating the Validity of ERT-derived Transport Parameters, *Vadose Zone J.*, *8*, 711-722.

Koestel, J. K., J. Moeys, and N. J. Jarvis (2011), Evaluation of Nonparametric Shape Measures for Solute Breakthrough Curves, *Vadose Zone J.*, *10*, 1261-1275.

Kohne, J. M., S. Kohne, and J. Simunek (2009), A review of model applications for structured soils: a) Water flow and tracer transport, *J. Contam. Hydrol.*, *104*, 4-35.

LaBrecque, D. J., and X. Yang (2001), Difference Inversion of ERT Data: a Fast Inversion Method for 3-D In Situ Monitoring, *J. Environ. Eng. Geophys.*, *6*, 83-89.

Larsson, M. H., and N. J. Jarvis (1999), A dual-porosity model to quantify macropore flow effects on nitrate leaching, *J. Environ. Qual.*, *28*, 1298-1307.

Lissner, H., et al. (2014), Degradation of deicing chemicals affects the natural redox system in airfield soils, *Environ. Sci. Pollut. Res.*, *21*, 9036-9053.

Looms, M. C., et al. (2008), Identifying unsaturated hydraulic parameters using an integrated data fusion approach on cross-borehole geophysical data, *Vadose Zone J.*, *7*, 238-248.

Loubet, B., et al. (2011), Carbon, nitrogen and Greenhouse gases budgets over a four years crop rotation in northern France, *Plant and Soil*, *343*, 109-137.

Luo, J., O. A. Cirpka, and P. K. Kitanidis (2006), Temporal-moment matching for truncated breakthrough curves for step or step-pulse injection, *Adv. Water Resour.*, *29*, 1306-1313.

Macduff, J. H., and R. E. White (1984), Components of the Nitrogen-Cycle Measured for Cropped and Grassland Soil-Plant Systems, *Plant and Soil*, *76*, 35-47.

Magesan, G. N., R. E. White, and D. R. Scotter (1996), Nitrate leaching from a drained, sheep-grazed pasture .1. Experimental results and environmental implications, *Australian Journal of Soil Research*, *34*, 55-67.

1055 Marchetti, R., G. Ponzoni, and P. Spallacci (2004), Simulating nitrogen dynamics in
1056 agricultural soils fertilized with pig slurry and urea, *J. Environ. Qual.*, *33*, 1217-1229.
1057 McCarthy, J. F., and L. D. McKay (2004), Colloid transport in the subsurface: Past, present,
1058 and future challenges, *Vadose Zone J.*, *3*, 326-337.
1059 Morales, V. L., J. Y. Parlange, and T. S. Steenhuis (2010), Are preferential flow paths
1060 perpetuated by microbial activity in the soil matrix? A review, *J. Hydrol.*, *393*, 29-36.
1061 Moysey, S., K. Singha, and R. Knight (2005), A framework for inferring field scale rock
1062 physics relationships through numerical simulation, *Geophys. Res. Lett.*, *32*, L08304.
1063 Munoz, F., R. S. Mylavarapu, and C. M. Hutchinson (2005), Environmentally responsible
1064 potato production systems: A review, *J. Plant Nutr.*, *28*, 1287-1309.
1065 NOAA (2013), National Oceanic and Atmospheric Administration: National Climatic Data
1066 Center, date accessed: October 2012. http://www.ncdc.noaa.gov/data-access/land-
1067 based-station-data/land-based-datasets/quality-controlled-local-climatological-data-
1068 qclcd.
1069 Nolan, B. T., et al. (1998), A National Look at Nitrate Contamination of Ground Water, *Water*
1070 *Conditioning and Purification*, *39*, 76-79.
1071 Oldenburg, D. W., and Y. G. Li (1999), Estimating depth of investigation in dc resistivity and
1072 IP surveys, *Geophysics*, *64*, 403-416.
1073 Olsen, P. A., et al. (1999), Characterizing solute transport in undisturbed soil cores using
1074 electrical and X-ray tomographic methods, *Hydrol. Process.*, *13*, 211-221.
1075 Onsoy, Y. S., et al. (2005), Spatial variability and transport of nitrate in a deep alluvial vadose
1076 zone, *Vadose Zone J.*, *4*, 41-54.
1077 Sanwald, K., and B. Wiseman (2008), ESN 44-0-0 fertilizer release time curves 2008/09,
1078 unpublished data, Cornell University Cooperative Extension of Suffolk County,
1079 Riverhead, US.
1080 Sanwald, K., and B. Wiseman (2012, 2013), Personal Communication, Cornell University
1081 Cooperative Extension of Suffolk County, Riverhead, US.
1082 Schmutz, M., et al. (2010), Influence of oil saturation upon spectral induced polarization of
1083 oil-bearing sands, *Geophys. J. Int.*, *183*.
1084 Simunek, J., et al. (2003), Review and comparison of models for describing non-equilibrium
1085 and preferential flow and transport in the vadose zone, *J. Hydrol.*, *272*, 14-35.
1086 Singha, K., F. D. Day-Lewis, and J. W. Lane (2007), Geoelectrical evidence of bicontinuum
1087 transport in groundwater, *Geophys. Res. Lett.*, *34*.
1088 Singha, K., et al. (2011), Quantifying solute transport processes: Are chemically
1089 "conservative" tracers electrically conservative?, *Geophysics*, *76*, F53-F63.

1090 Skiba, U., et al. (2009), Biosphere-atmosphere exchange of reactive nitrogen and
1091 greenhouse gases at the NitroEurope core flux measurement sites: Measurement
1092 strategy and first data sets, *Agric. Ecosyst. Environ.*, *133*, 139-149.
1093 Slater, L., et al. (2000), Cross-hole electrical imaging of a controlled saline tracer injection, *J.*
1094 *Appl. Geophys.*, *44*, 85-102.
1095 Slater, L., et al. (1997), Electrical Imaging of Saline Tracer Migration for the Investigation of
1096 Unsaturated Zone Transport Mechanisms, *Hydrol. Earth Syst. Sci.*, *1*, 291-302.
1097 Toride, N., F. J. Leij, and M. T. van Genuchten (1999), The CXTFIT code for estimating
1098 transport parameters from laboratory or field tracer experiments. Version 2.1 USDA
1099 Research Report, U. S. Salinity Laboratory, USDA, Riverside, CA.
1100 Ulrich, C., and L. D. Slater (2004), Induced polarization measurements on unsaturated,
1101 unconsolidated sands, *Geophysics*, *69*, 762-771.
1102 Van Breemen, N., et al. (2002), Where did all the nitrogen go? Fate of nitrogen inputs to
1103 large watersheds in the northeastern USA, *Biogeochemistry*, *57*, 267-293.
1104 Vanderborght, J., and H. Vereecken (2001), Analyses of locally measured bromide
1105 breakthrough curves from a natural gradient tracer experiment at Krauthausen, *J.*
1106 *Contam. Hydrol.*, *48*, 23-43.
1107 Velthof, G. L., et al. (2014), The impact of the Nitrates Directive on nitrogen emissions from
1108 agriculture in the EU-27 during 2000-2008, *Sci. Total Environm.*, *468*, 1225-1233.
1109 Vinegar, H. J., and M. H. Waxman (1984), Induced polarization of shaly sands, *Geophysics*,
1110 *49*, 1267-1287.
1111 Wang, Z., A. Tuli, and W. A. Jury (2003), Unstable Flow during Redistribution in
1112 Homogeneous Soil, *Vadose Zone J.*, *2*, 52-60.
1113 Wehrer, M., et al. (2014), Electrical resistivity tomography as monitoring tool for unsaturated
1114 zone transport: An example of preferential transport of deicing chemicals, *Environ.*
1115 *Sci. Pollut. Res.*, *21*, 8964-8980.
1116 Wehrer, M., and L. Slater (2015), Characterization of water content dynamics and tracer
1117 breakthrough by 3D electrical resistivity tomography (ERT) under transient
1118 unsaturated conditions *Water Resour. Res.*, *51*, 97-124.
1119 Weihermuller, L., et al. (2007), In situ soil water extraction: A review, *J. Environ. Qual.*, *36*,
1120 1735-1748.
1121 White, R. E., and A. N. Sharpley (1996), The fate of non-metal contaminants in the soil
1122 environment, in *Contaminants and the Soil Environment in the Australasia-Pacific*
1123 *Region*, edited by R. Naidu, pp. 29-67, Springer.
1124 Wyland, L. J., et al. (1996), Winter cover crops in a vegetable cropping system: Impacts on
1125 nitrate leaching, soil water, crop yield, pests and management costs, *Agric. Ecosyst.*
1126 *Environ.*, *59*, 1-17.

Zebarth, B. J., et al. (2012), Controlled release fertilizer product effects on potato crop response and nitrous oxide emissions under rain-fed production on a medium-textured soil, *Canadian Journal of Soil Science*, *92*, 759-769.

List of Figures

Figure 9: First central moments of the fertilizer experiment plotted versus the tracer experiment for the BTCs of nitrate and bromide, seepage water conductivity BTCs and ERT BTCs (from left to right). Different row numbers refer to the compartment rows of the MCS.

Figure 10: Variances of the BTCs of the three different methods plotted for the fertilizer experiment versus the tracer experiment.

Figure 11: Difference of the normalized first moments $\Delta\mu_1'$ between fertilizer experiment and tracer experiment observed in conductivity responses by ERT and seepage water plotted versus respective differences observed in BTCs of nitrate and bromide.

Table 1: Details of the infiltration events

infiltration no.	time since fertilizer application (d)	duration (h)	infiltrated amount (mm)	rate (mm h^{-1})	cumulative drainage (mm)
1	7	175	13.4	4.61	59
2	14	285	19.4	4.08	23
3	28	175	14.4	4.94	44
4	35	235	20.8	5.31	63
5	49	116	10.0	5.17	78
6	69	154	12.6	4.91	89
7	91	145	12.2	5.06	98
8	125	140	12.9	5.52	106
9	132	155	13.2	5.09	117
10	139	138	11.4	4.97	128
11	146	155	12.0	4.64	139
12	153	148	13.3	5.40	151
13	160	134	11.0	4.91	161
14	174	140	13.1	5.63	171
15	188	148	11.4	4.62	181
16	216	200	14.6	4.37	193
17	223	270	14.1	3.14	205
18	266	185	21.3	6.90	219
19	272	215	12.3	3.42	233
20	327	240	12.8	3.20	242
21	342	153	11.6	4.55	251
22	350	150	12.6	5.04	262

Table 2: solution compositions for PHREEQC calculations. Ionic strength and electrical conductivity σ_w and ion balance error are results of the simulation.

solution 1: seepage water compositions	Minimum[1)]	Maximum[2)]	hypothetical minimum source zone concentration[3)]	solution 2: nitrification reaction	hypothetical minimum source zone concentration[4)]	hypothetical maximum source zone concentration[5)]
Ca^{2+} (mmol/l)	1.36	3.66	29.31	Ca[6)] (mmol/l)	2.70	2.70
Cl^- (mmol/l)	4.64	4.37	34.97	$Cl^{-6)}$ (mmol/l)	5.40	5.40
K^+ (mmol/l)	0.37	0.51	4.08	Urea[7)] (mmol/l)	0.14	90.00
Mg^{2+} (mmol/l)	1.33	3.43	27.45	H^+ (mmol/l)	0.29	178.90
NO_3^- (mmol/l)	1.56	11.39	91.14	NO_3^- (mmol/l)	0.29	179.90
Na^+ (mmol/l)	0.65	0.49	3.94			
ionic strength (mmol/l)	8.98	22.57	180.60		8.38	187.00
σ_w (µS/cm)	668	1544	10619		778	65585
% ion balance error	1.38	-1.83				

[1)] Concentrations of the seepage water at minimum electrical conductivity

[2)] Concentrations of the seepage water at maximum electrical conductivity

[3)] 8-fold concentration of maximum seepage water concentrations; conservative estimate based on 7-fold dilution of Br- Tracer pulse observed by [*Wehrer and Slater*, 2015]

[4)] estimate based on similar ionic strength as minimum seepage water composition

[5)] estimate based on similar ionic strength as 8-fold maximum seepage water composition

[6)] from input solution

[7)] urea is consumed in the reaction, so it is not present in the final solution; also hydrogen carbonate is not present due to low pH

Table 3: correlation coefficients.

μ_1' s.w.c.	μ_1' nitrate	0.95
μ_1' ERT	μ_1' nitrate	0.79
μ_1' ERT	μ_1' s.w.c.	0.86
μ_1' nitrate	μ_1' bromide	0.82
μ_1' s.w.c. fertilizer	μ_1' s.w.c. tracer	0.70
μ_1' ERT fertilizer	μ_1' ERT tracer	0.54
μ_2' s.w.c.	μ_2' nitrate	0.73
μ_2' ERT	μ_2' nitrate	0.46
μ_2' ERT	μ_2' s.w.c.	0.58
μ_2' nitrate	μ_2' bromide	*-0.18*
μ_2' s.w.c. fertilizer	μ_2' s.w.c. tracer	*-0.10*
μ_2' ERT fertilizer	μ_2' ERT tracer	*-0.06*
max s.w.c.	max nitrate	0.92
max ERT	max nitrate	0.85
max ERT	max s.w.c.	0.87
area s.w.c.	area nitrate	0.96
area ERT	area nitrate	0.90
area ERT	area s.w.c.	0.90
$\Delta\mu_1'$ s.w.c.	$\Delta\mu_1'$ nitrate-bromide	0.81
$\Delta\mu_1'$ ERT	$\Delta\mu_1'$ nitrate-bromide	0.78
$\Delta\mu_1'$ ERT	$\Delta\mu_1'$ s.w.c.	0.71
$\Delta\mu_2'$ s.w.c.	$\Delta\mu_2'$ nitrate	0.56
$\Delta\mu_2'$ ERT	$\Delta\mu_2'$ nitrate	0.64
$\Delta\mu_2'$ ERT	$\Delta\mu_2'$ s.w.c.	0.47

s.w.c.: seepage water conductivity; max: maximum; Δ-values refer to the differences of moments between tracer and fertilizer experiment; all correlations, except the ones in italics, are significant at the p= 0.01-level.

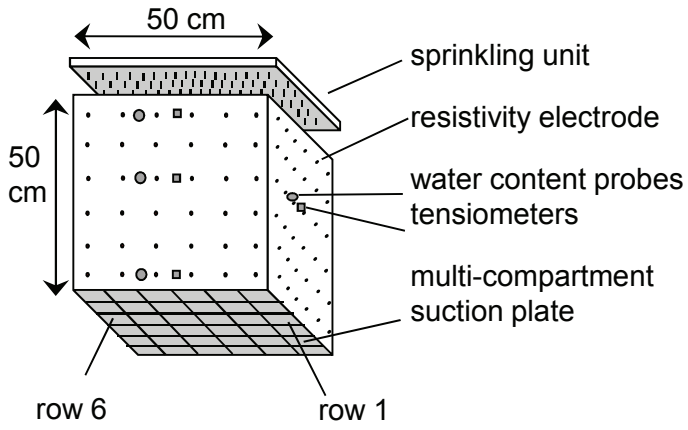
50 cm
50
cm
sprinkling unit
resistivity electrode
water content probes
tensiometers
multi-compartment
suction plate
row 6
row 1

Figure 1

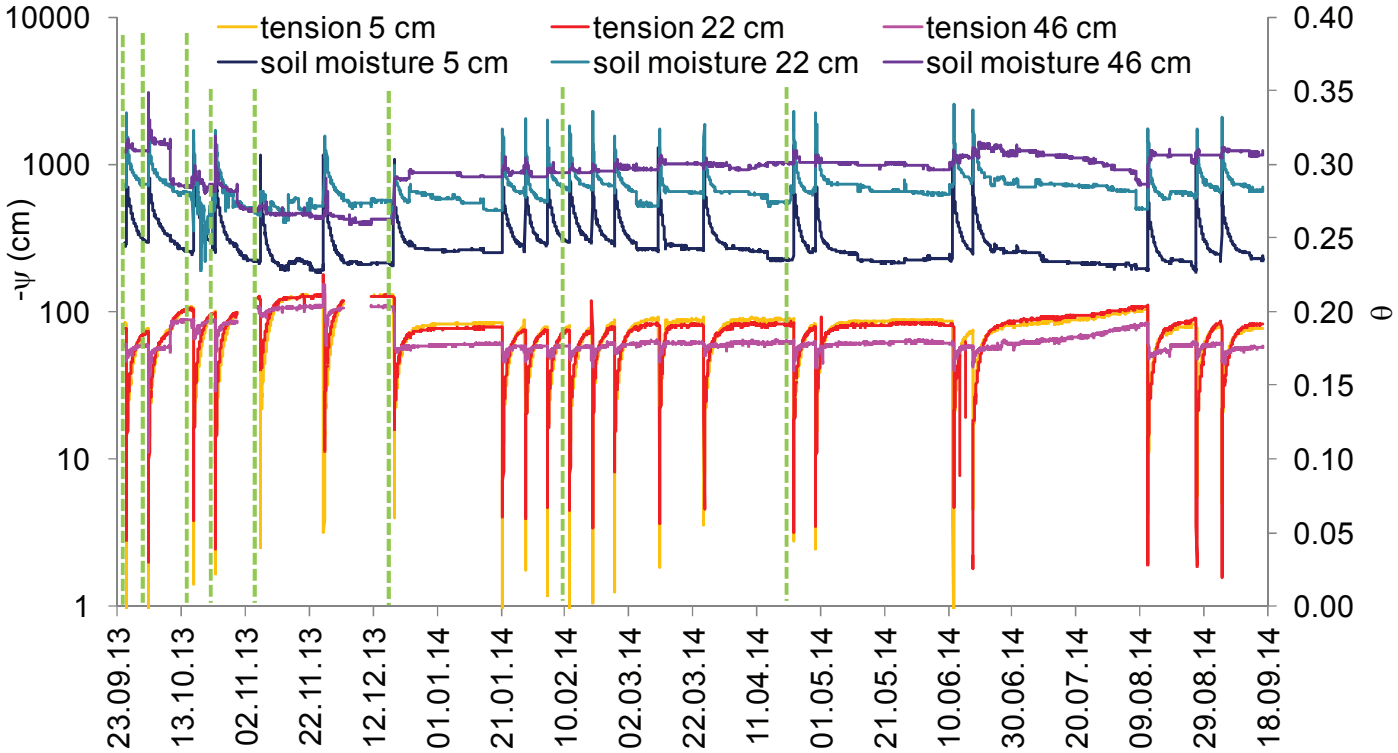
tension 5 cm
tension 22 cm
tension 46 cm
soil moisture 5 cm
soil moisture 22 cm
soil moisture 46 cm
10000
1000
100
10
1
-ψ (cm)
0.40
0.35
0.30
0.25
0.20
0.15
0.10
0.05
0.00
θ
23.09.13
13.10.13
02.11.13
22.11.13
12.12.13
01.01.14
21.01.14
10.02.14
02.03.14
22.03.14
11.04.14
01.05.14
21.05.14
10.06.14
30.06.14
20.07.14
09.08.14
29.08.14
18.09.14

Figure 2

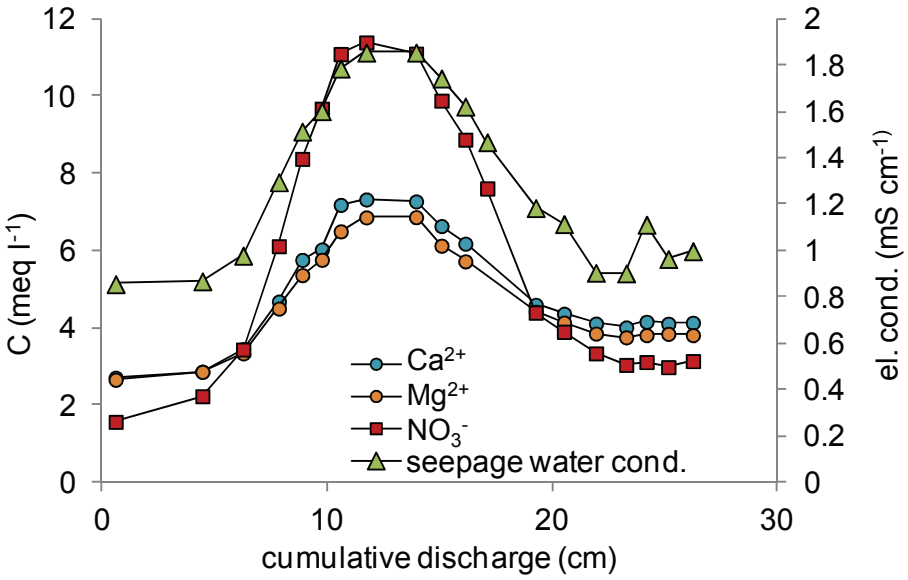
12
10
8
6
4
2
0
C (meq l-1)
2
1.8
1.6
1.4
1.2
1
0.8
0.6
0.4
0.2
0
el. cond. (mS cm-1)
0
10
20
30
cumulative discharge (cm)
Ca2+
Mg2+
NO3-
seepage water cond.

Figure 3

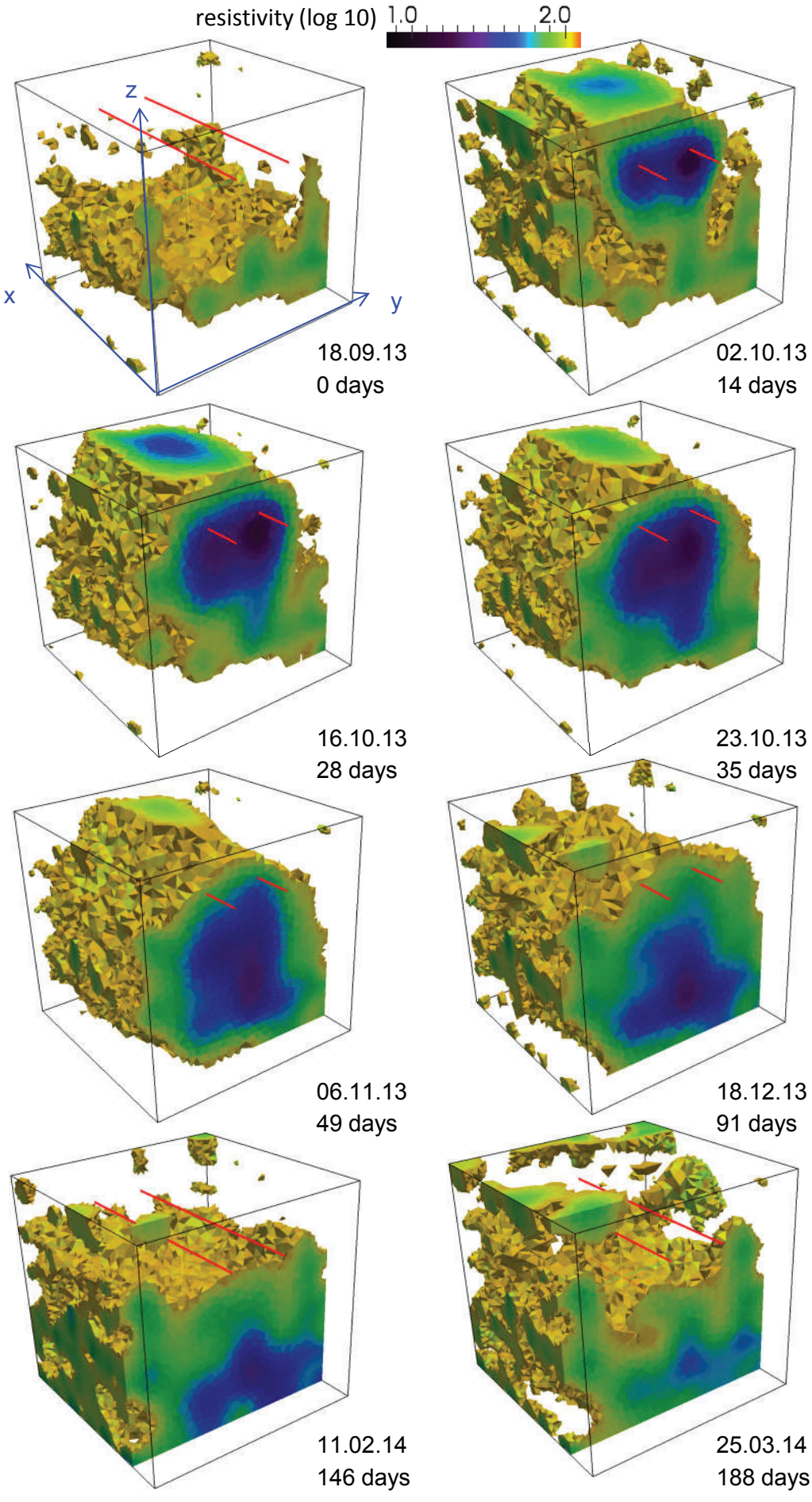
resistivity (log 10)
1.0
2.0
z
x
y
18.09.13
0 days
02.10.13
14 days
16.10.13
28 days
23.10.13
35 days
06.11.13
49 days
18.12.13
91 days
11.02.14
146 days
25.03.14
188 days

Figure 4

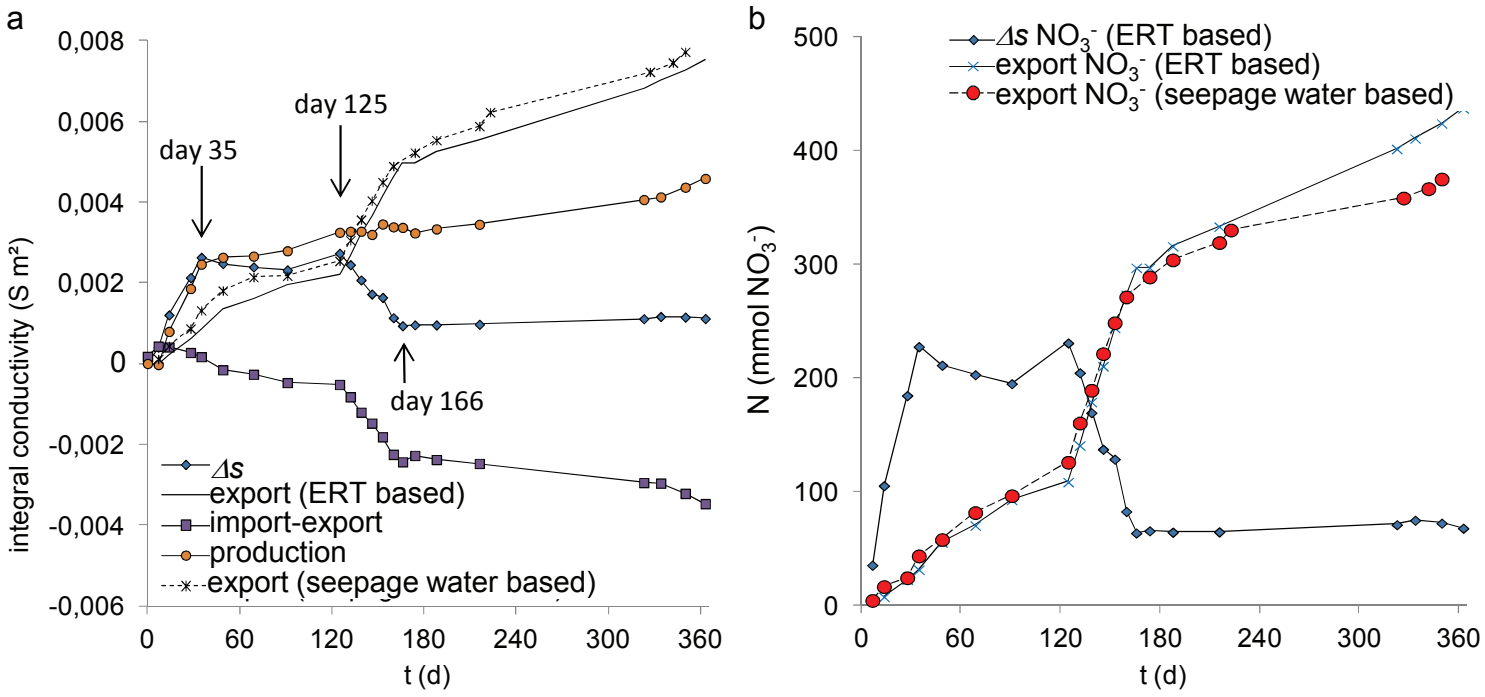
a
0,008
0,006
0,004
0,002
0
-0,002
-0,004
-0,006
integral conductivity (S m²)
day 35
day 125
day 166
Δs
export (ERT based)
import-export
production
export (seepage water based)
0
60
120
180
240
300
360
t (d)
b
500
400
300
200
100
0
N (mmol NO3-)
Δs NO3- (ERT based)
export NO3- (ERT based)
export NO3- (seepage water based)
0
60
120
180
240
300
360
t (d)

Figure 5

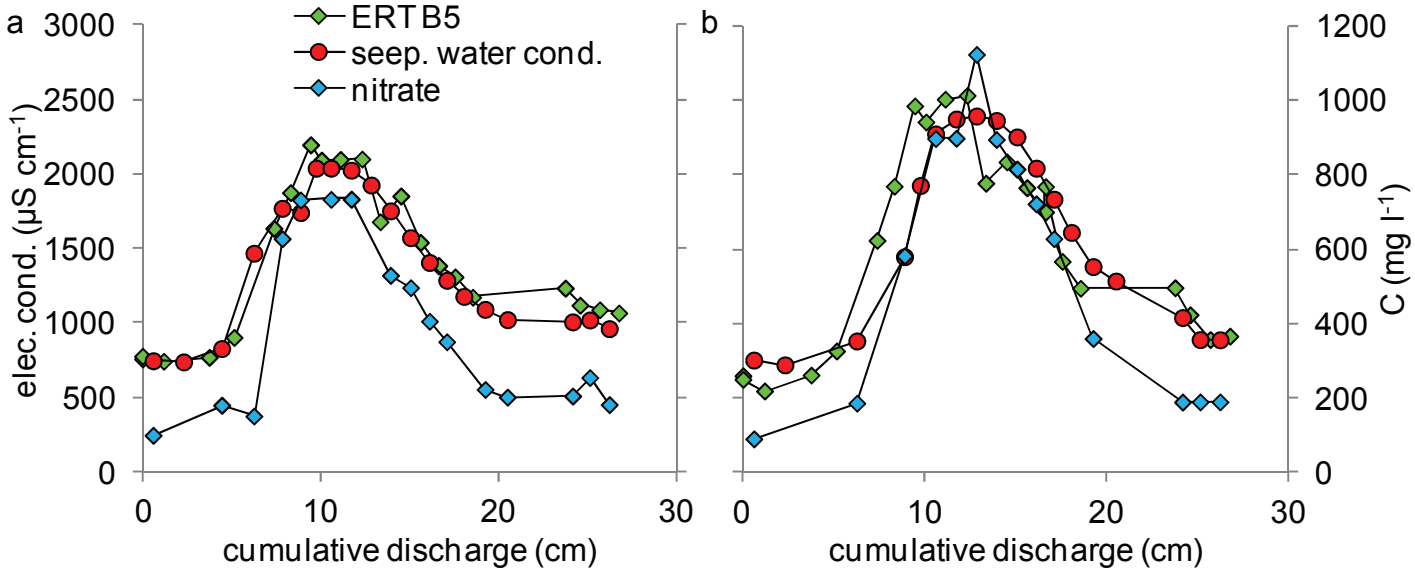
a
b
ERT B5
seep. water cond.
nitrate
elec. cond. (µS cm-1)
C (mg l-1)
cumulative discharge (cm)
cumulative discharge (cm)
0
500
1000
1500
2000
2500
3000
200
400
600
800
1000
1200
10
20
30

Figure 6

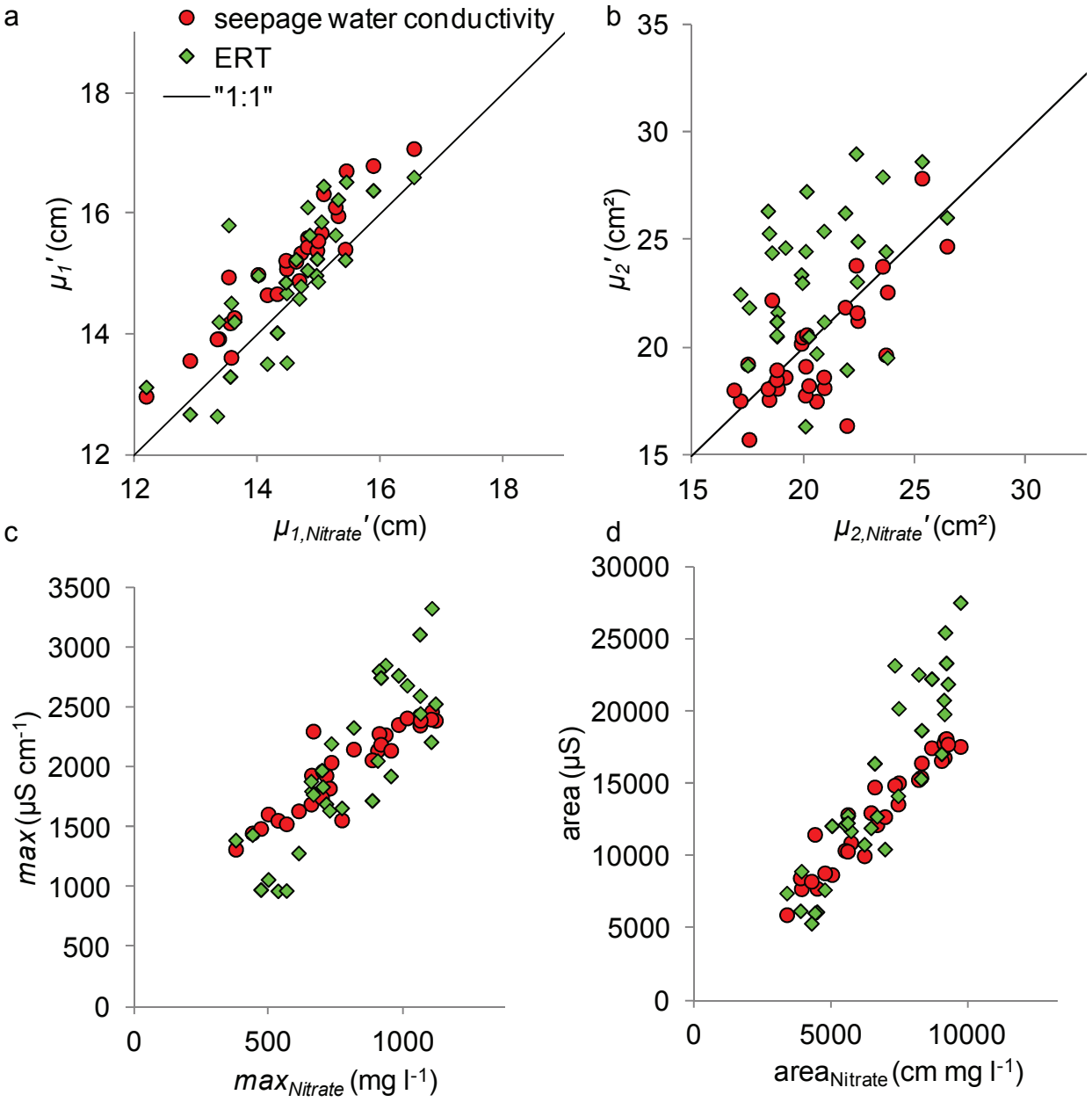
a
seepage water conductivity
ERT
"1:1"
18
16
14
12
12
14
16
18
μ1' (cm)
μ1,Nitrate' (cm)
b
35
30
25
20
15
15
20
25
30
μ2' (cm²)
μ2,Nitrate' (cm²)
c
3500
3000
2500
2000
1500
1000
500
0
0
500
1000
max (µS cm-1)
maxNitrate (mg l-1)
d
30000
25000
20000
15000
10000
5000
0
0
5000
10000
area (µS)
areaNitrate (cm mg l-1)

Figure 7

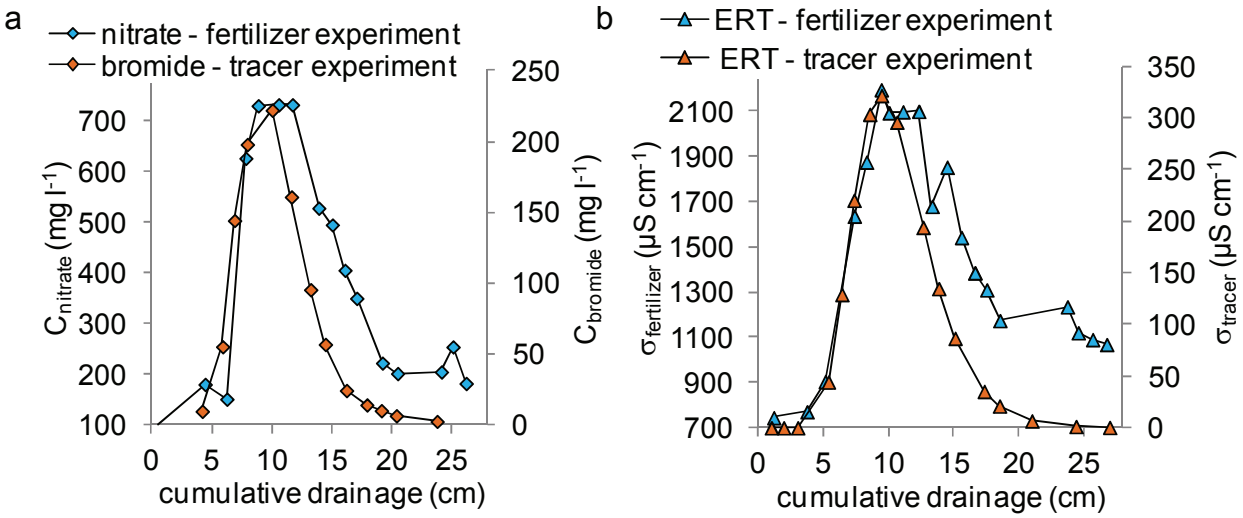
a
nitrate - fertilizer experiment
bromide - tracer experiment
C nitrate (mg l-1)
C bromide (mg l-1)
cumulative drainage (cm)
b
ERT - fertilizer experiment
ERT - tracer experiment
σ fertilizer (µS cm-1)
σ tracer (µS cm-1)
cumulative drainage (cm)

Figure 8

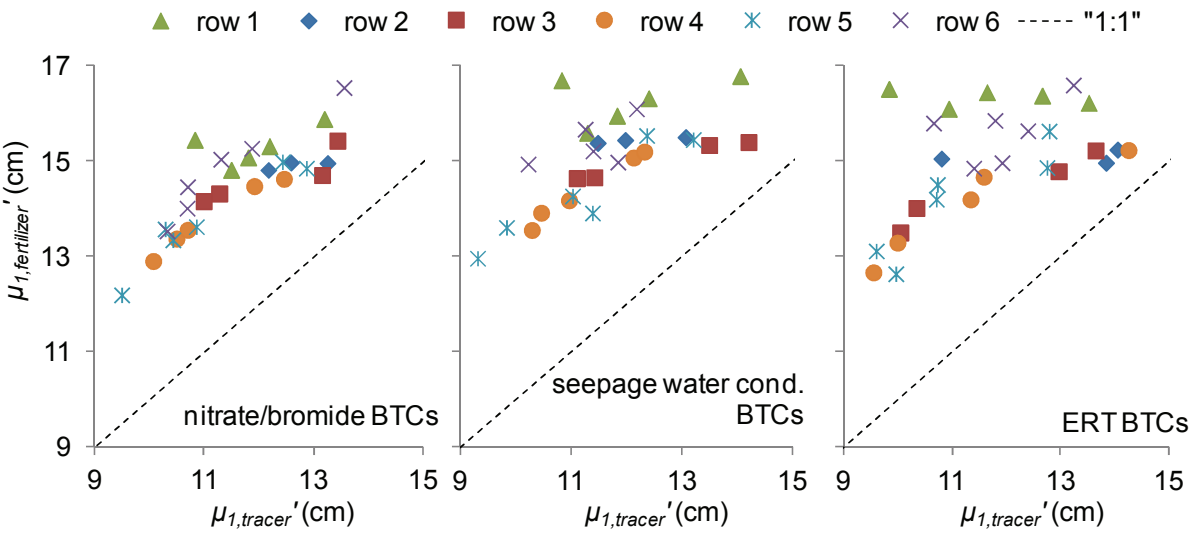
row 1
row 2
row 3
row 4
row 5
row 6
"1:1"
17
15
13
11
9
$\mu_{1,fertilizer}'$ (cm)
nitrate/bromide BTCs
seepage water cond. BTCs
ERT BTCs
9
11
13
15
$\mu_{1,tracer}'$(cm)

Figure 9

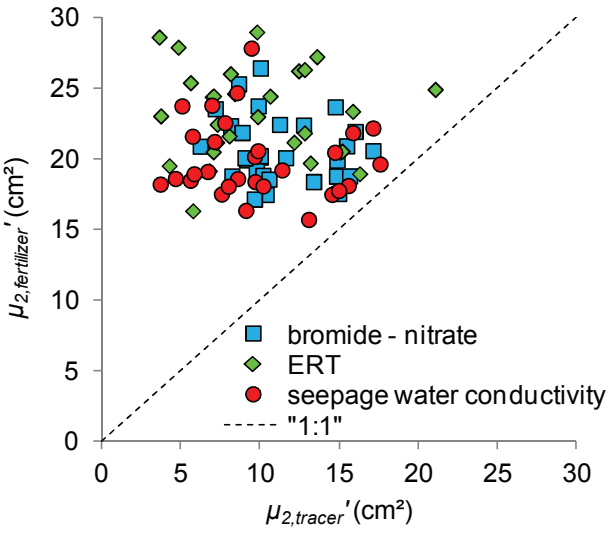
30
25
20
15
10
5
0
0
5
10
15
20
25
30
$\mu_{2,fertilizer}'$ (cm²)
$\mu_{2,tracer}'$ (cm²)
bromide - nitrate
ERT
seepage water conductivity
"1:1"

Figure 10

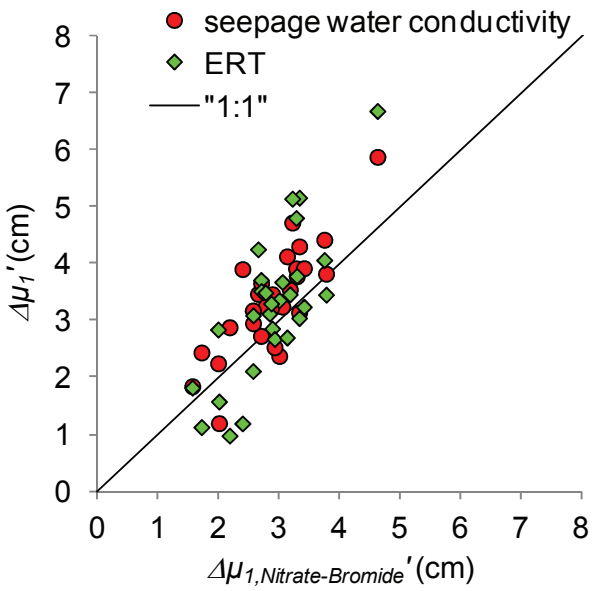
seepage water conductivity
ERT
"1:1"
8
7
6
5
4
3
2
1
0
0
1
2
3
4
5
6
7
8
Δμ1'(cm)
Δμ1,Nitrate-Bromide'(cm)

Figure 11